REVIEW PAPER

# Advances in electrokinetics and their applications in micro/nano fluidics

**Cunlu Zhao · Chun Yang**

**Abstract** Electrokinetic phenomena originally developed in colloid chemistry have drawn great attention in micro- and nano-fluidic lab-on-a-chip systems for manipulation of both liquids and particles. Here we present an overview of advances in electrokinetic phenomena during recent decades and their various applications in micro- and nano-fluidics. The advances in electrokinetics are generally classified into two categories, namely electrokinetics over insulating surfaces and electrokinetics over conducting surfaces. In each category, the phenomena are further grouped according to different physical mechanisms. For each category of electrokinetics, the review begins with basic theories, and followed by their applications in micro- and/or nano-fluidics with highlighted disadvantages and advantages. Finally, the review is ended with suggested directions for the future research.

**Keywords** Electrokinetic phenomena ·
Micro- and nano-fluidics · Surface-charge modulation ·
Induced-charge electrokinetics

## 1 Introduction

The manipulation of fluids and particles at microscale level is receiving intensive attention due to its relevance to the development of micro total analysis systems (μTAS) for drug screening and delivery, environmental and food monitoring, biomedical diagnoses and chemical analyses,

etc. However, the widely used fluid manipulation techniques at macroscale cannot be directly adopted at microscale due to the inherently small Reynolds number involved in microscale. One typical example is that the fluid instabilities caused by inertial effects at macroscale disappear at microscale due to strong viscous effects. Thus, the microfluidic mixing is dominated by molecular diffusion, without much benefit of the flow instabilities. In fluidic devices with micrometer scales (10–100 μm), it takes relatively long time (e.g., about 100 s for molecules with diffusivity of $10^{-10}$ m$^2$/s) to achieve a good mixing. Another inherent limitation at microscale is that the pressure-driven flow becomes inefficient, because the flow rate under a given driving pressure gradient is inversely proportional to the fourth power of channel dimension. Various techniques are thus being proposed for pumping, mixing, manipulating, and separating liquids and particles at microscales. Owing to large surface to volume ratios in microfluidic devices, surface phenomena naturally are among the most preferred ones. Electrokinetic phenomena belong to such surface phenomena, and already become the most popular non-mechanical techniques in microfluidic devices. The popularity of electrokinetic techniques is ascribed to their numerous advantages: no moving parts and thus immune to mechanical failure, readily electronic control and thus ease of automation, flat velocity profiles of liquid sample and thus effectively reduce the sample dispersion, fluid or particle velocity does not depend on the microchannel dimensions, etc..

Since the fluid or particle velocity generated by conventional electrokinetics is linearly proportional to the strength of externally applied electric field, the conventional electrokinetic phenomena are also termed linear electrokinetic phenomena. The classic electrokinetic phenomena, however, have some drawbacks (Bazant and

C. Zhao · C. Yang (✉)
School of Mechanical and Aerospace Engineering,
Nanyang Technological University, 50 Nanyang Avenue,
Singapore 639798, Singapore
e-mail: mcyang@ntu.edu.sg

Squires 2004): (1) the poor control of surface charge (or zeta potential); (2) the resulting velocity for liquid or particle is somewhat low, e.g., $u_s = 70$ μm/s in aqueous solution with $E_0 = 100$ V/cm and $\zeta = 10$ mV; (3) AC electric fields that can reduce undesirable electrochemical reactions produce no net motion of liquid or particle. Some of recently developed electrokinetic techniques are of proven ability to diminish or circumvent one or some of these disadvantages rooted in classic linear electrokinetics.

This paper reviews development in electrokinetics by focusing on physical mechanisms as well as micro- and/or nanofluidic applications. This review is organized as follows: Section 2 presents basic theories for the electric double layer and classic electrokinetic phenomena since they are helpful to understand the advances in electrokinetics reviewed later. Section 3 reviews comprehensively the development in electrokinetic phenomena and their micro- and/or nanofluidic applications. In Sect. 4, the conclusions are made and possible research directions for future studies are identified and highlighted.

## 2 Classic electrokinetic phenomena

### 2.1 The classic theory of electric double layer (EDL)

Solid surfaces acquire electrical charges when they are brought into contact with polar solvents (Hunter 1981) such as electrolyte solution. The origins of such surface charges are diverse, including several popular mechanisms: (1) preferential adsorption of ions in the solution, (2) adsorption–desorption of lattice ions, (3) direct dissociation or ionization of surface groups, and (4) charge-defective lattice: isomorphous substitution.

To maintain the electroneutrality of the system, electric double layer (EDL) with excess of counterions must be formed to counterbalance the surface charge. Although it is traditionally termed "double" layer, its structure can be very complicated and may contain three or more layers in most instances. Figure 1 below illustrates schematically the most general model for an electrical double layer. For example, consider in this case that the surface charge is negative and a layer of some anionic species (green) in the solution is specifically absorbed on the surface. Such specific absorption is mainly due to the chemical affinity of ionic species to the solid surface other than Coulombic interactions (Delgado et al. 2007; Hunter 1981). Outside the layer of specifically absorbed ions, counterions (cations) are attracted by the negatively charged surface due to the Coulombic force only.

Based on the Gouy–Chapman–Stern model shown in Fig. 1, the structure of EDL can be identified as follows (Delgado and Arroyo 2002; Delgado et al. 2007):
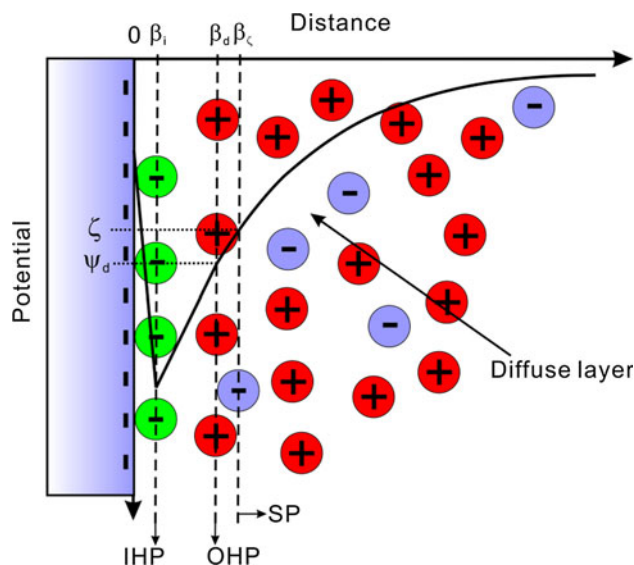


**Fig. 1** Schematic illustration of the Gouy-Chapman-Stern model for an electric double layer (EDL) of a negatively charged interface

(i)   The plane located at $x = \beta_i$ is called the inner Helmholtz plane (IHP) and the plane at $x = \beta_d$ is called the outer Helmholtz plane (OHP). The IHP is the plane cutting through the center of the adsorbed species. The OHP is the plane cutting through the counterions at their position of closest approach.

(ii)  The region between $x = 0$ and $x = \beta_d$ is often named the Stern layer or sometimes the compact part of the double layer.

(iii) The portion extending from $x = \beta_d$ is called the diffuse layer or sometimes the diffuse part of the double layer. The concentration of counterions in the diffuse layer decreases as the location departs away from the surface.

(iv)  The plane located at $x = \beta_\zeta$ is called the shear plane (SP). The well-known zeta potential is defined as the potential difference between this plane and the bulk solution. In general, SP is not co-planar with OHP. At the SP, it is assumed that the viscosity of the liquid medium jumps discontinuously from infinity in the Stern layer to a finite value in the diffuse layer. Shear plane is the boundary that separates the EDL into a mobile part and an immobile part. For the sake of convenience, the zeta potential is taken to be equivalent to the potential at the OHP in most circumstances, i.e. $\psi_d = \zeta$. See page 201–216 in Hunter (1981) for more detailed discussion.

The OHP signifies the beginning of the diffuse layer. The diffuse layer can be mathematically described in terms of the equilibrium condition for ions as

$$-ez_i\nabla\psi - k_B T\nabla\ln n_i = 0 \tag{1}$$

where $e$ is the elementary charge, $z_i$ denotes the valence of ions, $k_B$ is the Boltzmann constant, $T$ is the absolute temperature, and $n_i$ is the number concentration of ions. In Eq. (1), the first term corresponds to the electrostatic force on ions of type $i$ and the second term denotes the thermodynamic force due to ionic diffusion. The solution of Eq. (1) under the condition $n_i = n_i^0(\infty)$ for $\psi = 0$ leads to the famous Boltzmann distribution

$$n_i(\mathbf{r}) = n_i^0(\infty)\exp\left[-\frac{ez_i\psi(\mathbf{r})}{k_B T}\right] \tag{2}$$

where $n_i^0(\infty)$ is the bulk number concentration of ions of type $i$ (far from the charged surface), and vector $\mathbf{r}$ represents the location in the electrolyte domain. Finally, the Poisson equation relates the potential and ionic concentrations by

$$\nabla^2\psi(\mathbf{r}) = -\frac{1}{\varepsilon_0\varepsilon_r}\rho(\mathbf{r})$$
$$= -\frac{1}{\varepsilon_0\varepsilon_r}\sum_{i=1}^{N}ez_i n_i^0(\infty)\exp\left[-\frac{ez_i\psi(\mathbf{r})}{k_B T}\right] \tag{3}$$

where $\varepsilon_0$ is the electric permittivity of vacuum ($8.854 \times 10^{-12}$ F/m) and $\varepsilon_r$ is the dielectric constant of electrolyte solution. In most related studies of electrokinetics, the dielectric constant of electrolyte solution ($\varepsilon_r$) is assumed to be constant in the whole electrolyte domain. Equation (3) is the so-called Poisson–Boltzmann equation which is the mathematical presentation of Gouy–Chapman theory describing the physics of the diffuse part of EDL.

Due to non-linearity, there is no general solution to this partial differential equation, but in certain cases analytical solutions are available.

*Case 1* For a flat surface with a low potential $\psi_d$, Eq. (3) can be linearized based on the Debye-Hückel approximation, and then the solution can be sought as

$$\psi = \psi_d e^{-\kappa x} \tag{4}$$

where $\kappa^{-1}$ is called the Debye length which gives a measure of the thickness of the EDL. It can be formulated as

$$\lambda_D = \kappa^{-1} = \sqrt{\frac{\varepsilon_0\varepsilon_r k_B T}{\sum_{i=1}^{N}e^2 z_i^2 n_i^0(\infty)}} \tag{5}$$

the typical values of Debye length $\kappa^{-1}$ for different electrolyte concentrations for the case of binary monovalent electrolytes are shown in Table 1. It is clear that the Debye length decreases with increasing the electrolyte concentration. At high molarities, the thickness of EDL is very small. However, the double layer thickness in a solution without electrolytes can be regarded as infinitely thick (i.e., a large distance from the surface).

**Table 1** Relationship between molar concentration and Debye length for binary monovalent electrolytes at 25°C

| Ionic concentration, M | Debye length $\kappa^{-1}$, nm |
| --- | --- |
| $10^{-6}$ | 304 |
| $10^{-4}$ | 30.4 |
| $10^{-2}$ | 3.04 |

*Case 2* For a flat surface with an arbitrary potential $\psi_d$ and a symmetric electrolyte ($z_1 = -z_2 = z$), the Poisson–Boltzmann Eq. (3) has the famous Gouy–Chapman solution given by

$$Y(x) = 2\ln\left[\frac{1 + e^{-\kappa x}\tanh(Y_d/4)}{1 + e^{-\kappa x}\tanh(Y_d/4)}\right] \tag{6}$$

where $Y$ is the dimensionless potential

$$Y = \frac{ze\psi}{k_B T} \tag{7}$$

*Case 3* For a spherical surface (radius $a$) with low potentials, Eq. (3) can be solved as

$$\psi(r) = \psi_d\left(\frac{a}{r}\right)e^{-\kappa(r-a)} \tag{8}$$

For other cases, either numerical solutions or approximate methods have to be applied to solve Eq. (3).

2.2 Classic linear electrokinetic phenomena

Generally speaking, electrokinetic phenomena are the consequences of the interaction between applied electric field and the EDL. In the context of classic electrokinetics, surface charges are solely determined by the physiochemical properties of the surface and solution. Therefore, for a given surface and electrolyte solution, the surface charge is fixed and independent of external electric field.

*2.2.1 Small zeta potentials*

A solid surface submerged in aqueous solutions acquires a charge density $q$ which attracts counterions and repels co-ions to form an EDL (effectively a surface capacitor). The diffuse ionic charge in the EDL gradually screens the electric field generated by the surface charge, resulting in an electric potential drop across the EDL (which effectively represents the zeta potential). Under the Debye–Hückel linear approximation (small surface charge or potential), the potential in the diffuse part of double layer is given by Eq. (4) from which one can obtain a linear relationship between the surface charge density ($q$) and the zeta potential ($\zeta$) as

$$q = \zeta\varepsilon_0\varepsilon_r\kappa \tag{9}$$

Two popular electrokinetic phenomena are electro-osmosis and electrophoresis; both find myriads of

microfluidic applications for chemical analyses, biomedical diagnostics, and colloidal particle manipulations. Electroosmotic flows occur along charged solid walls subject to a tangential electric field. The externally applied electric field exerts an electrostatic body force on the net charge density in the diffuse part of EDL, driving the ions and the liquid in the EDL into motion. Subsequently, the momentum generated inside the EDL gradually diffuses to the bulk liquid due to the viscous coupling. At the steady state, the velocity of the bulk liquid reaches a uniform value and the resulting fluid flow appears to slip at the outer edge the EDL with thickness of $\lambda_D$ (as shown in Fig. 2a). Such slip velocity is given by the Helmholtz–Smoluchowski equation

$$u_s = -\frac{\varepsilon_0 \varepsilon_r \zeta}{\mu} E_0 \tag{10}$$

where $\mu$ is the fluid viscosity and $E_0$ is the strength of applied electric field. In microfluidic applications where the thin EDL assumption applies, it is evident that the velocity of electroosmosis does not depend on the channel dimensions. This unique feature is strikingly different from the pressure-driven flow in which the velocity depends strongly on channel dimensions. Consequently, the electroosmotic pumping has long been an efficient and popular technique for fluid transportation in microfluidic devices. On the other hand, for a charged particle freely suspended in an electrolyte solution, the electroosmotic slip velocity over the particle surface gives rise to particle motion opposite to the electroosmotic slip velocity, known as electrophoresis (as shown in Fig. 2b). Under the thin double layer limit, the electrophoretic velocity of particle is given by the Smoluchowski equation

$$U = \frac{\varepsilon_0 \varepsilon_r \zeta}{\mu} E_0 = \mu_{EP} E_0 \tag{11}$$

where $E_0$ is the strength of external electric field, and $\mu_{EP} = \varepsilon_0 \varepsilon_r \zeta / \mu$ is called the electrophoretic mobility of the particle (Note that $\zeta$ is the particle zeta potential). More comprehensive and detailed descriptions of classic electrokinetics are provided in textbooks and reviews (Anderson 1989; Ghosal 2004; Hunter 1981; Masliyah and Bhattacharjee 2006; Probstein 1994; Russel et al. 1989).

### 2.2.2 Large zeta potentials

If a solid surface is so heavily charged that the zeta potential becomes comparable to or much larger than the so-called thermal voltage, $k_B T/(ze)$, the exponential profile of EDL potential given by Eq. (4) and the linear zeta potential–surface charge relation given by Eq. (9) become invalid. The potential in the diffuse part of double layer satisfies the non-linear Poisson–Boltzmann equation and the solution is given by Eq. (6). Under the thin double layer limit, one can obtain a non-linear surface charge–potential relation for the double layer of a symmetric, binary electrolyte from Eq. (6) as

$$q = 4n_0 ze \lambda_D \sinh\left(\frac{ze\zeta}{2k_B T}\right) \tag{12}$$

It should be noted here that $q$ generally grows exponentially with $ze\zeta/(k_B T)$. For heavily charged surfaces, the result predicted from Eq. (12) significantly deviates from that predicted from Eq. (9). For weakly charged surfaces, it is not surprising that Eq. (12) can reduce to Eq. (9) by using the famous Debye–Hückel linear
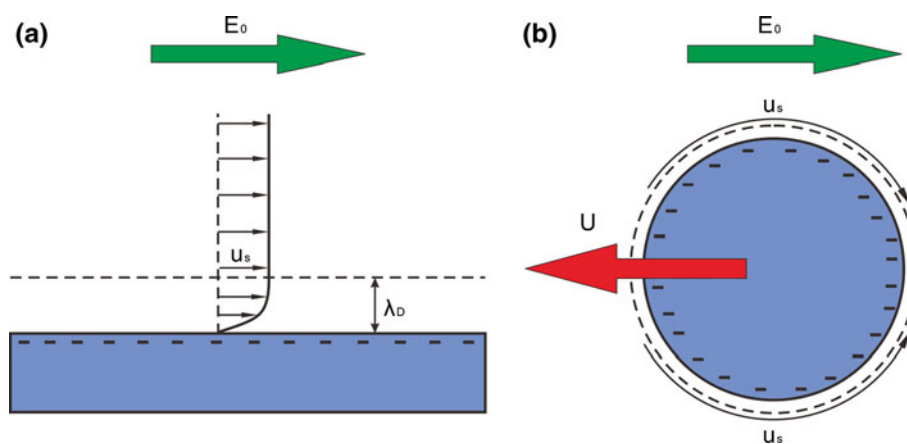


Fig. 2 a Electroosmosis: an electric double layer (EDL) of thickness $\lambda_D$ is formed over a negatively charged solid surface submerged in an electrolytic solution. A tangentially applied electric field exerts electrostatic forces on the mobile ions in the EDL to result in electroosmotic slip flow over the charged surface. b Electrophoresis:

Under an electric field, a freely suspended charged particle in an electrolyte solution moves with a velocity equal in magnitude and opposite in direction to the electroosmotic slip velocity on the particle surface

approximation, $\sinh[\mathrm{ze}\zeta/(2k_\mathrm{B}T)] \approx \mathrm{ze}\zeta/(2k_\mathrm{B}T)$. It also has been pointed out that the nonlinearity defined by Eq. (12) would have important implications for double layer relaxation (Bazant et al. 2004). In such non-linear regime, the Helmholtz–Smoluchowski Eq. (10) for the electroosmotic slip is still valid on condition that (Squires and Bazant 2004)

$$\frac{\lambda_\mathrm{D}}{a}\exp\left(\frac{\mathrm{ze}\zeta}{2k_\mathrm{B}T}\right) \ll 1 \qquad (13)$$

where $a$ denotes the radius of surface curvature. For the situations involving thick EDLs and/or large zeta potentials, Eq. (13) is violated and ionic concentrations in the EDL are significantly different from their bulk values. Then the surface conduction inside the EDL becomes significant and its effects on electrokinetics must be taken into account. For example, the electrophoretic mobility, $\mu_\mathrm{EP}$, becomes dependant non-linearly on the dimensionless Dukhin number,

$$\mathrm{Du} = \frac{\sigma_s}{\sigma a} \qquad (14)$$

which characterizes the ratio of the surface conductivity, $\sigma_\mathrm{s}$, to the bulk conductivity, $\sigma$ (Lyklema 1995).

Both electromigration and convective transport of ions in the EDL contribute to the surface conductance, $\sigma_\mathrm{s}$. The relative importance of convective transport is characterized by another dimensionless number $m = 2\varepsilon_0\varepsilon_\mathrm{r}[k_\mathrm{B}T/(\mathrm{ze})]^2/(\mu D)$ ($D$ is diffusion coefficient of ions) and the formula for Du takes a simple form for a symmetric binary electrolyte (Squires and Bazant 2004)

$$\begin{aligned}\mathrm{Du} &= \frac{2\lambda_\mathrm{D}(1+m)}{a}\left[\cosh\left(\frac{\mathrm{ze}\zeta}{2k_\mathrm{B}T}\right) - 1\right] \\ &= 4\frac{\lambda_\mathrm{D}(1+m)}{a}\sinh^2\left(\frac{\mathrm{ze}\zeta}{2k_\mathrm{B}T}\right)\end{aligned} \qquad (15)$$

In the extreme cases of infinitely thin double layers ($\lambda_\mathrm{D} \rightarrow 0$), the condition expressed by Eq. (13) is satisfied and the Dukhin number disappears naturally, so the electrophoretic mobility is exactly given by the Smoluchowski Eq. (10). For highly charged particles ($\zeta \gg k_\mathrm{B}T/(\mathrm{ze})$) with finite double layer thickness, however, the Dukhin number is generally of finite values and the surface conduction plays significant roles. The direct consequences of surface conduction are the generation of bulk concentration polarization and a non-uniform diffuse charge distribution around the particle, which would add diffusiophoretic and concentration polarization contributions to electrophoretic mobility of the particle. One can refer to Dukhin (1993) and Lyklema (1995) for more detailed discussion of surface conduction.

# 3 Advances in electrokinetic phenomena

In classic electrokinetic phenomena, solid surfaces possess homogeneous constant surface charge (or zeta potential). When the solid surfaces acquire inhomogeneous zeta potentials, interesting and useful phenomena can occur. Based on the polarizability of surfaces over which electrokinetic phenomena take place, we generally divide the electrokinetics into two categories: electrokinetics involving non-polarizable surfaces and electrokinetics involving polarizable surfaces.

## 3.1 Non-polarizable (insulating) surfaces

Although the application of externally driving electric field does not influence the surface charge on insulating surfaces in classic linear electrokinetic phenomena, variation of the surface charge still can be realized through different techniques.

### 3.1.1 Electrokinetic phenomena with surface charge patterning

In the classical electrokinetic phenomena, a fixed, homogeneous surface charge (or, zeta potential $\zeta$) is widely assumed. Electrokinetic phenomena over surfaces with inhomogeneously patterned surface charges/potentials have been reported in the literature. Anderson and Idol (1985) found that flow circulations exist in the electroosmotic flow through inhomogeneously charged pores. By modulating the surface charge density on the walls of a microchannel, it was shown that a net electroosmotic flow can be controlled to be either parallel or perpendicular to the externally applied field (Ajdari 1995; Stroock et al. 2000). Figure 3 schematically illustrates the principle of electroosmotic flow control in microchannels by surface charge modulation. These ideas have been further realized to fabricate a "transverse electrokinetic pump" which has an advantageous feature that it can be powered by low voltages applied across a narrow channel (Gitlin et al. 2003). By modulation of both the channel geometry and the surface charge, Ajdari (2001) introduced a large class of transverse electrokinetic effects which could be exploited for fabrication of micropumps, micromixers, and flow detectors.

To visualize the flow patterns of electroosmosis, a caged-fluorescence technique was developed to measure the fluid velocity and sample-dispersion rate of electroosmosis in cylindrical capillaries with a non-continuous distribution of zeta potential (Herr et al. 2000). The adsorption of analyte molecules also can cause the channel wall to be
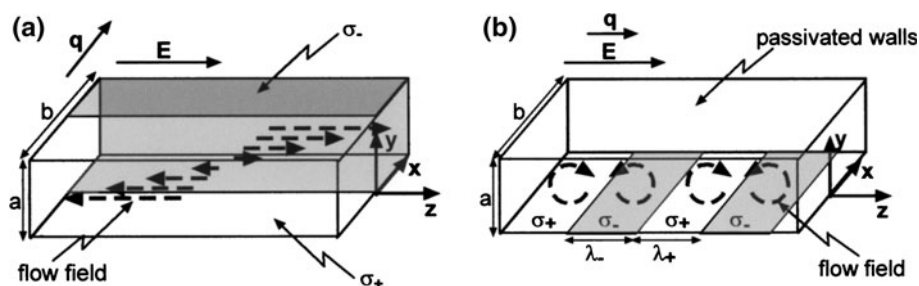
**Fig. 3** Mechanisms of surface charge modulation in microchannels. $\sigma_+$ and $\sigma_-$ represent the positive and negative surface charge densities respectively. $q$ represents the direction of surface charge variation. The *dotted arrows* represent the electroosmosis generated in the channel. **a** $q \perp E$: The direction of surface charge variation is

perpendicular to the applied electric field: positive surface charge density $\sigma_+$ on one half domain ($x < 0$) and negative surface charge density $\sigma_-$ on the other half domain ($x > 0$). **b** $q \| E$: The direction of surface charge variation is parallel to the applied electric field (Stroock et al. 2000)

inhomogeneously charged, and the resulting electroosmosis has been shown to increase the analyte dispersion that can decrease the resolution in capillary electrophoresis (Ghosal 2003; Long et al. 1999). Brotherton and Davis (2004) elaborated the effects of step changes in both zeta potential and cross section on electroosmosis in slit channels with arbitrary shapes of cross section. Their analyses indicated that the flow pattern in each region is a combination of an electroosmotic flow and a pressure-driven flow. Halpern and Wei (2007) theoretically examined the electroosmotic flow in a microcavity patterned with nonuniform surface charge. The results showed that the flow demonstrates various patterns, depending on the aspect ratio of the cavity and the distribution of zeta potential. Zhang and Qiu (2008) demonstrated both experimentally and numerically the generation of 3D vortices by patterning surface with discrete charge patches on the inner surface of a round capillary tube. Lee et al. (2011) conducted a 3-D numerical study to investigate how the solute dispersion during electroosmotic migration is affected by the variation of surface and solution properties in microchannels. It was found that the dispersion rate of a solute plug is increased by shear flows generated by zeta potential variations across and along the microchannel.

The surface charge modification can also be used to tune the electrophoretic motion of particles. Teubner (1982) was the very first to investigate the electrophoresis of particles with inhomogeneous zeta potentials. However, the details of electrophoretic characteristics were not elaborated. For a colloidal particle with spatially inhomogeneous zeta potentials, Anderson (1985) demonstrated interesting and counter-intuitive effects that not only the total net charge but also the distribution of surface charge affects electrophoretic mobility of the colloidal particle. Long and Ajdari (1998) theoretically examined the electrophoresis of colloids with patterned shape and surface charge, and found that patterned colloids undergo a pure motion of rotation or move transversely to the applied electric field. Figure 4 presents an
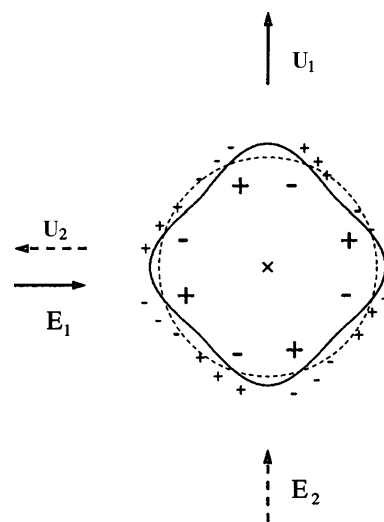


**Fig. 4** Electrophoretic motion of a cylinder with both patterned shape $a(\theta) = 1[1 + \alpha \cosh(4\theta)]$ and surface charge $q(\theta) = q_0 \cos(4\theta + \pi/2)$. The direction of the cylinder motion is always perpendicular to the direction of applied electric field (Long and Ajdari 1998)

example with both patterned shape and surface charge. The patterned shape and surface charge in this case are defined by $a(\theta) = a_0[1 + \alpha \cosh(4\theta)]$ and $q(\theta) = q_0 \cos(4\theta + \pi/2)$, respectively. $a_0$ is the cylinder radius at $\theta = \pi/8$ (i.e., the radius for the original circular cylinder denoted by the *dash line*), $\alpha$ is a small perturbation to the original circular cross-section, and $q_0$ represents the surface charge density at $\theta = -\pi/8$.

The surface charge patterning was also adopted in nanofluidics to achieve nanofluidic diodes (Daiguji et al. 2005; Karnik et al. 2007; Vlassiouk et al. 2008; Yan et al. 2009). Such nanofluidic diodes simulate semiconductor diodes widely used in electronics and thus demonstrate the ionic current rectification which can turn ionic current on and off by changing the polarity of the applied electric field (see Fig. 5). Ionic rectifying effect relies on overlapped
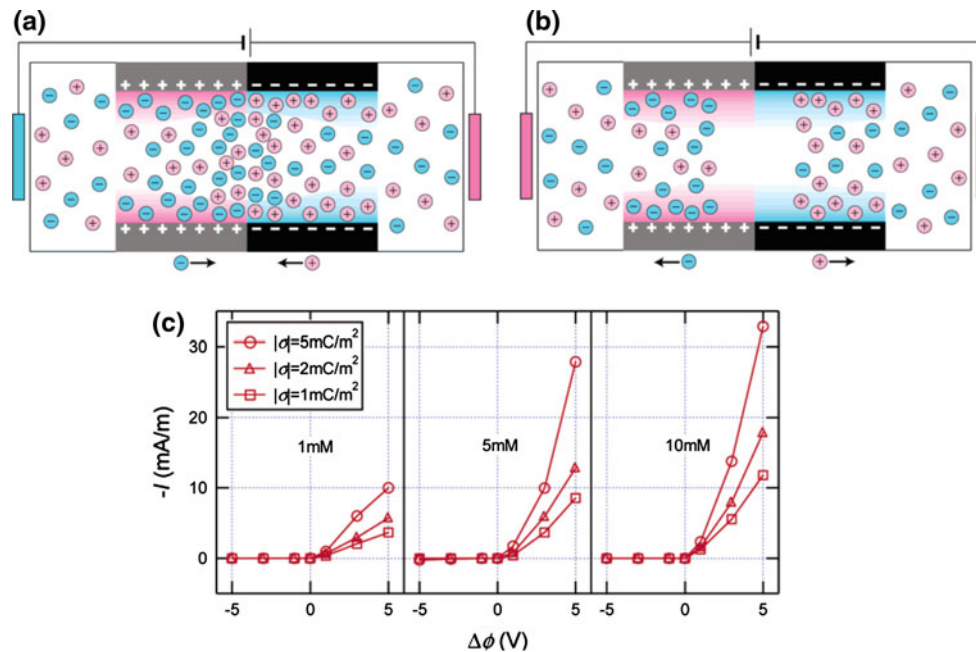
**Fig. 5** Working principle of a nanofluidic diode utilizing a nanochannel with half positively charged wall and half negatively charged wall. In case (**a**), the voltage is applied from the negatively charged wall to the positively charged wall (positive voltage), cations and anions are both concentrated to the middle of the nanochannel, leading to enhanced ionic conductance and large electric current. While in case (**b**), the voltage is applied from the positively charged wall to the negatively charged wall (negative voltage), cations and anions are both depleted from the nanochannel, leading to reduced ionic conductance and negligible electric current. The corresponding current–potential relationship is presented in (**c**) which clearly shows the behavior of ionic rectification (Daiguji et al. 2005)

EDLs and inhomogeneous surface charge. Therefore, such effect is unique to nanofluidics and cannot be present in microfluidics. Other than surface charge patterning, geometric asymmetry of nanochannels with uniformly charged walls (Macrae et al. 2010; Perry et al. 2010; Siwy 2006; Vlassiouk and Siwy 2007) and a combination of surface charge pattering and geometric asymmetry of nanochannel (Constantin and Siwy 2007; Yan et al. 2009) also can induce rectifying effects of ionic current. More comprehensive description of nanofluidic diodes can be found in a recent review by Cheng and Guo (2010).

### 3.1.2 Electrokinetic phenomena with active surface charge modulation

Another variation of surface charge can be achieved actively by applying electric field perpendicularly to the solid surface. Lee et al. (1990) first applied this technique to manipulate zeta potential of capillary wall for improving the separation efficiency in capillary electrophoresis. In their system, an auxiliary side electrode was embedded inside the capillary wall to set up an electric field that can modify the wall zeta potential. Ghowsi and Gale (1991) demonstrated the feasibility of electroosmosis control in a similar configuration. By analogy with the electronic field-effect transistor (FET), Schasfoort et al. (1999) further developed microfluidic flow FETs based on the same

concept. Flow FETs, whose working mechanism is illustrated in Fig. 6, employ an additional electrode embedded behind the insulating channel wall to establish a modulating electric field which maintains a non-zero potential difference between this auxiliary electrode and the bulk fluid. Active control of such non-zero potential difference modifies the potential drop across the EDL (so-called effective zeta potential), which in turn alters the electro-osmotic flow. Van Der Wouden et al. (2006) demonstrated that directional flow can be induced in an AC field-driven microfluidic FET by the synchronized switching of the gate potential and the channel axial potential.

Following the applications of FET to manipulate electroosmotic flows in microchannels, Daiguji et al. (2003) and Daiguji et al. (2005) theoretically extended the field-effect control to nanofluidics. They showed that the FET technique can be used to regulate ionic transport by locally modifying the surface charge density on the nanochannel walls when the EDLs are overlapped. Karnik et al. (2005) experimentally demonstrated the use of field effect control in nanofluidics. They showed that the gate voltage modulates the charge on the nanochannel walls and thus ionic conductance, which holds the promise for development of integrated nanofluidic circuits with applications in manipulating ions and biomolecules. Figure 7 shows a typical FET configuration for modulating ionic charge inside a nanochannel. The ionic charge can be readily controlled by
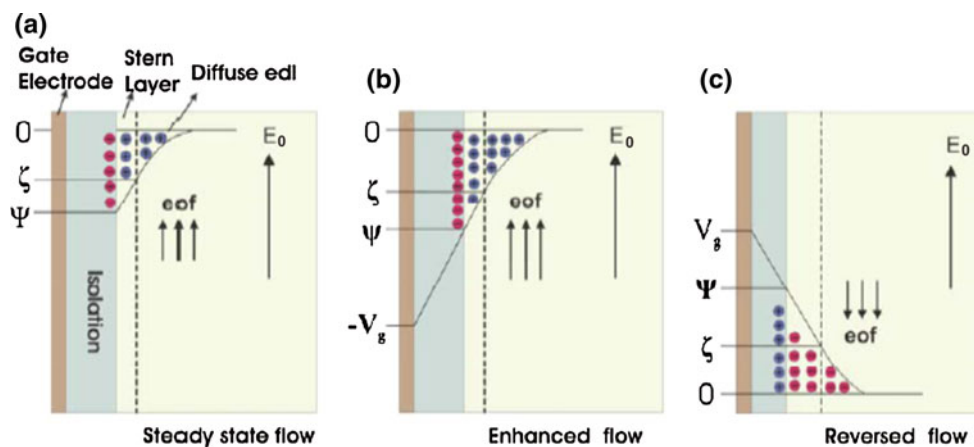
**Fig. 6** Schematic representation of the operation principle of a flow FET. Although the driving electric field $E_0$ is fixed, the direction and intensity of electroosmotic flow can be adjusted by a gate voltage which modulates the local zeta potential. In Case (**a**), there is no applied gate voltage and the velocity of electroosmotic flow is proportional to the natural zeta potential. In case (**b**), an applied negative gate voltage $V_g$ enhances the negative zeta potential and thus the electroosmotic flow. In case (**c**), a positive gate potential reverses the charge in the EDL and thus the electroosmotic flow (Schasfoort et al. 1999)
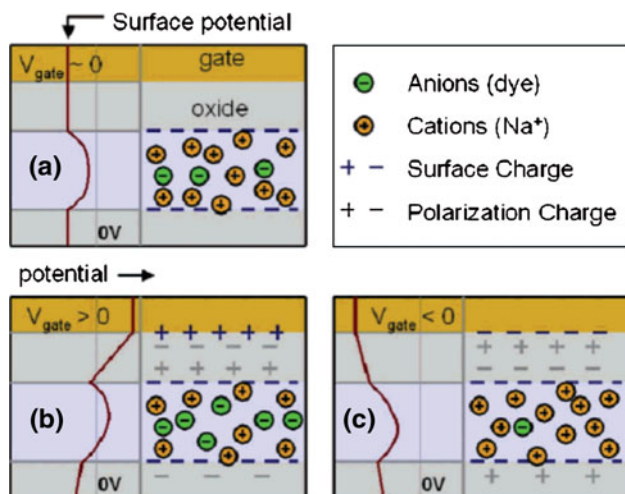


**Fig. 7** Schematic mechanisms of charge modulation inside a nanochannel by using the FET technique. **a** In the absence of the gate voltage $V_{gate} = 0$, the nanochannel mainly contains cations due to the natural negative surface charge. **b** With a positive gate voltage $V_{gate} > 0$, cations are depleted and anions are concentrated. **c** With a negative gate voltage $V_{gate} < 0$, cations are concentrated and anions are depleted (Karnik et al. 2005)

varying the gate voltage, allowing for dynamic and electronic control of ionic transport through a nanochannel. Later, transport of proteins through nanochannels (Karnik et al. 2006) and protons inside silica films (Fan et al. 2008) as well as the ionic conductance and rectification in nanochannels (Fan et al. 2005; Guan et al. 2011; Joshi et al. 2010) were also modulated utilizing the same gate control technique.

The effectiveness of FET flow control method has been demonstrated with both fused-silica capillaries and microfabricated channels. This method demonstrates a higher level of controllability because of its ability of modifying surface charge or zeta potential dynamically and electrically. However, in such typical FET configuration, an insulation layer usually separates the gate electrode from the fluid, and high gate voltages are required to modulate zeta potential or surface charge of the channel wall for producing effective FET effects. For example, as reported by Sniadecki et al. (2004), for modification of the surface charge density of the channel, gate voltages in a range of $-120$ to $+120$ V were applied across a parylene C layer of 1.22 μm thickness sandwiched between the fluid and the gate electrode. Similarly, Schasfoort et al. (1999) applied a transverse voltage of 50 V across a 390 nm thick insulation layer made of silicon nitride to alter the surface charge density for controlling an electroosmotic flow.

Moorthy et al. (2001) introduced another active way of surface charge control. The method relies on $TiO_2$-coated walls whose zeta potential can be modified via the UV light exposure.

### 3.1.3 Electrokinetic phenomena with hydrophobic surfaces

Nowadays, more microfluidic devices are fabricated using hydrophobic materials, such as polydimethylsiloxane (PDMS) and poly (methyl methacrylate) (PMMA). Molecular dynamic simulations suggest that the conventional non-slip boundary condition becomes invalid because of the hydrophobicity of solid surface, and the liquid appears to slip on the solid surface (Barrat and Bocquet 1999a, b). The widely used hydrodynamic boundary condition accounting for such hydrodynamic slip was proposed by Navier (1823) who assumed that the slip velocity on the solid surface $u_s$ is linear proportional to the rate of shear on the solid surface, i.e., $u_s = b(\partial u/\partial y)|_{y=0}$,

where $u$ is fluid velocity profile, $y$ is the coordinate normal to the surface (see Fig. 8). The coefficient of proportionality $b$ denotes the slip length which measures the distance between the solid surface and an imaginary surface where the slip velocity on solid surface is linearly extrapolated to zero. Experimentally, it has been already confirmed that the slip length for smooth and homogeneous hydrophobic surfaces is limited to several tens of nanometers (Chiara et al. 2005; Cottin-Bizonne et al. 2005; Craig et al. 2001; Lasne et al. 2008; Olga 1999; Vinogradova et al. 2009; Zhu and Granick 2001, 2002). Since the contribution of hydrodynamic slip on flow enhancement is determined by the ratio of slip length to the scale of the channel in pressure-driven flows (Eijkel 2007), the slip-induced flow enhancement is insignificant for pressure-driven microfluidic applications.

However, electroosmotic flows on smooth hydrophobic surfaces with nanometric slip lengths were found to be considerably enhanced (Ajdari and Bocquet 2006; Joly et al. 2004; Muller et al. 1986; Park and Kim 2009; Yang and Kwok 2003). A simple analysis of the electroosmosis over a hydrophobic surface with a small zeta potential $\zeta$ and a slip length $b$ results in a modified Helmholtz–Smoluchowski slip velocity (Zhao and Yang 2012)

$$u_{\mathrm{s}} = -\left(1 + \frac{b}{\lambda_{\mathrm{D}}}\right)\frac{\varepsilon_0\varepsilon_{\mathrm{f}}E_0\zeta}{\mu} \tag{16}$$

where $\varepsilon_0\varepsilon_{\mathrm{f}}$ and $\mu$ are the electric permittivity and dynamic viscosity of the electrolyte solution, respectively, and $E_0$ is the external electric field tangential to the hydrophobic surface. A comparison between Eqs. (16) and (10) indicates that the electroosmotic flow over slip hydrophobic surfaces is amplified by a factor of $1 + b/\lambda_{\mathrm{D}}$ as compared to the electroosmotic flow over no-slip hydrophilic surfaces. Since the Debye length measuring the thickness of EDL and the slip length $b$ are comparable and both in the
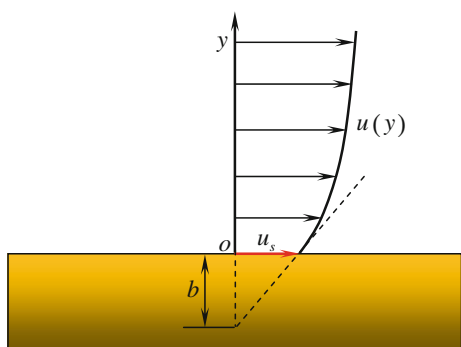
nanometer range, the significant enhancement of electroosmotic flow over smooth hydrophobic surfaces should be expected. Similarly, the concept of hydrodynamic slip was also extended for enhancing the electrophoretic mobility of particles (Khair and Squires 2009), the efficiency of electrokinetic energy conversion in nanochannels (Davidson and Xuan 2008; Goswami and Chakraborty 2009; Ren and Stein 2008) and the ionic transport in nanochannels (Vermesh et al. 2009). Previous reviewed works all assumed homogenous slip over solid surfaces, and another possibility may involve variation of hydrodynamic slip along solid surfaces. With patterned hydrodynamic slip on microchannel walls, the conventional plug flow profile of electroosmosis was found to be perturbed by the flow transversal to microchannel walls (Zhao and Yang 2012). Furthermore, if both hydrodynamic slip and electrokinetic effects are present in pressure-driven flows, Zhao and Yang (2011c) identified that there is a competition between the hydrodynamic slip effect and the electrokinetic effect, and thus there exists a critical slip length only above which the pressure-driven flows are enhanced while under which the pressure-driven flows are inhibited.

Another recent interest is liquid flows over superhydrophobic surfaces. The superhydrophobic surfaces display the so-called lotus-leaf effect which highly repels water. Different from the smooth hydrophobic surfaces, superhydrophobic surfaces are rough, which facilitates the trap of gas bubbles. For the typical Cassie state shown in Fig. 9, the gas is trapped in grooves and the liquid only rests on the top of the rough structures. The trapped gas bubbles immensely enhance hydrophobicity of the surface, giving rise to contact angels even larger than 175° (Bocquet and Barrat 2007). Hydrodynamically, the superhydrophobic surface with groove roughness shown in Fig. 9 usually leads to a no-slip boundary condition on the solid–liquid interface and a perfect slip boundary condition ($b = \infty$) on the liquid–gas interface. The trapped gas bubbles would
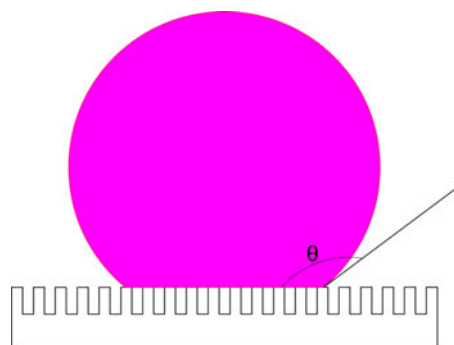


**Fig. 8** Hydrodynamic slippage over a hydrophobic surface. The liquid slip over a hydrophobic surface with velocity $u_{\mathrm{s}}$ which is linearly proportional to the local rate of shear $\partial u/\partial y|_{y=0}$, and the resulting proportionality defines the slip length $b$ over which the slip velocity is linearly extrapolated to zero



**Fig. 9** Superhydrophobic surface with a water droplet at the Cassie sate. The solid surface is rough with alternating grooves. The water droplet only rests on the tops of the roughness and the gas is trapped in the grooves, leading to a very large contact angle $\theta$

tremendously reduce the flow friction, and introduce very large effective slip lengths even several orders higher than slip lengths over smooth hydrophobic surfaces. For superhydrophobic surfaces with carefully designed roughness patterns, the apparent slip length can reach up to several microns (Joseph et al. 2006; Ou et al. 2004; Tsai et al. 2009) which can greatly enhance pressure-driven flows.

Only very recently, a number of theoretical studies were conducted to investigate the electroosmotic flow over superhydrophobic surfaces (Bahga et al. 2010; Belyaev and Vinogradova 2011; Squires 2008; Zhao 2010). It was shown that the electroosmotic flow over superhydrophobic surfaces is complicated by the charge and the hydrodynamic slip at the liquid–gas interface. The existing investigations generally reveal three scenarios for the electroosmotic flow over superhydrophobic surfaces: (1) if the liquid–gas interface is uncharged, the flow is negligibly enhanced or sometimes even retarded as compared to the flow over no-slip smooth surfaces (Bahga et al. 2010; Belyaev and Vinogradova 2011; Huang et al. 2008; Squires 2008). (2) if the liquid–solid and liquid–gas interfaces are similarly charged, the flow can be enhanced considerably by several orders of magnitude (Bahga et al. 2010; Belyaev and Vinogradova 2011; Squires 2008). (3) if the liquid–solid and liquid–gas interfaces are oppositely charged, the prediction suggests a reversed electroosmotic flow that can be present over the superhydrophobic surfaces with zero net charge (Belyaev and Vinogradova 2011). The above investigations assumed weakly charged surfaces and thus the effect of surface conduction is certainly negligible. However, for strongly charged surfaces (or large zeta potentials), surface conduction becomes important as suggested by Eq. (15) and its effect on the electroosmotic flows over superhydrophobic surfaces must be addressed.

Zhao (2010) extended former analyses to the strongly charged surfaces and found that considerable electroosmotic flow enhancement predicted previously for the weakly charge superhydrophobic surfaces could be significantly compressed by the non-uniform surface conduction due to the mismatch of ionic transport inside EDLs over no-slip and perfect-slip (or no-shear) regions. Figure 10 schematically illustrates generation of non-uniform surface conduction over a superhydrophobic surface and implications it could have on electroosmotic flows.

### 3.2 Polarizable (conducting) surfaces

When polarizable surfaces are subject to external electric field, the external driving electric field induces surface polarization charge in addition to the physiochemical bond charge on the surfaces, which would bring extra effects on classic electrokinetic phenomena. Depending on the locations where the phenomena arise (either on energized electrodes or around conductors floating in electric field), this category of electrokinetic phenomena can be classified as (i) AC electric field driven electrokinetic phenomena and (ii) induced-charge electrokinetic phenomena. Furthermore, another type of related electrokinetic phenomena termed electrokinetic phenomena of the second kind caused by the induced bulk charge around conducing surfaces is also reviewed here.

#### 3.2.1 AC electric field driven electrokinetic phenomena

A typical phenomenon in this subcategory allows for steady electroosmotic flows driven by AC electric field over two coplanar electrodes (see Fig. 11). This "AC electroosmosis (ACEO)" was first theoretically and
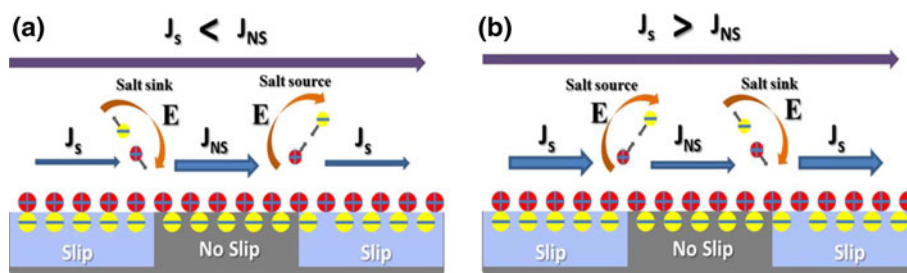


**Fig. 10** Mechanisms for non-uniform surface conduction on a superhydrophobic surface with alternating groove structures. In general, surface conduction over a superhydrophobic surface is inhomogeneous because of different hydrodynamic and charged conditions on liquid–solid and liquid–gas interfaces. In particular, for case (**a**), surface conduction over the solid surface is higher than that over the gas surface, $J_{NS} > J_S$, and consequently surface conduction current jumps at the junction connecting the solid and gas surfaces. To maintain the current continuity, electric current from the bulk over the left gas interface must go into the EDL over the solid surface, while electric current from the EDL over the solid surface much go

into the bulk over the right gas surface. These two electric currents from/into the bulk make the electric field penetrate into the EDL, rather than tangential to the double layer for the case without the inhomogeneous surface conduction. Therefore, the tangential component of the electric field inside the double layer is weakened, and the enhancement of electroosmotic flows due to the slip is much smaller than that predicted previously for the situation without accounting for the inhomogeneity of surface conduction. For case (**b**), surface conduction over the solid surface is lower than that over the gas surface, $J_{NS} < J_S$, the similar conclusions can be obtained (Zhao 2010)
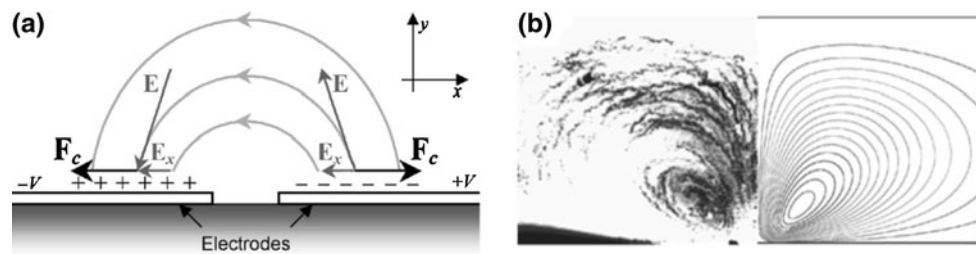
**Fig. 11** AC electroosmosis over two symmetric coplanar electrodes. **a** An EDL is induced over each electrode when coplanar electrodes are powered by an AC electric field with a particular frequency, and the induced EDLs can alter the external driving field. The electrostatic interaction of the EDLs with the local driving field gives rise to two opposite body forces which drive the AC electroosmosis. **b** A comparison between the measured streamlines on the *left* and the calculated streamlines on the *right* for the steady AC electroosmotic flow. If the electric field oscillates too slowly, the induced EDLs can fully screen the external driving field, resulting in zero AC electroosmosis. On the other hand, if the electric field oscillates too fast, the EDLs do not have time to form and AC electroosmosis also can disappear. Consequently, AC electroosmosis is strongest at a given field frequency (Green et al. 2002)

experimentally explored around a pair of adjacent, flat electrodes deposited on a glass slide and subjected to an AC driving field. The resultant basic flow patterns involve two counter-rotating vortices (Ramos et al. 1998, 1999). In the later serial papers (González et al. 2000; Green et al. 2000, 2002), detailed experimental, theoretical, and numerical analyses of ACEO on microelectrodes were performed. Figure 11 shows a classical configuration of ACEO system and a comparison between the experimental results and the theoretical predictions. The planar electrodes deposited on an insulating substrate are in contact with an infinite large domain of electrolyte solution (or confined by a microchannel), and ACEO is strongest at a certain applied frequency (González et al. 2000; Ramos et al. 1999). When two planar electrodes are integrated into a nanochannel with overlapped EDLs, the ACEO also can be induced by applying low AC voltages on the two electrodes, and was shown to be an effective way for pumping both ions and liquid solution (Sparreboom 2009; Talapatra and Chakraborty 2008). However, the existence of multiple characteristic frequencies instead of one complicates the phenomenon (Sparreboom 2009).

Meanwhile, ACEO was also implemented to achieve various microfluidic applications. Ajdari (2000) theoretically predicted the AC electroosmosis over asymmetric electrodes, and he pointed out that the pumping effect can be induced due to the symmetry breaking of electrode arrangement. Based on the same idea, prototypes of AC electrokinetic micropumps were constructed and analyzed (Mpholo et al. 2003; Ramos et al. 2003). AC electroosmosis was also utilized for rapid concentration of bioparticles (Wu et al. 2005), which can potentially lead to enhanced sensitivity of detection. Sasaki et al. (2006) introduced an AC electroosmotic flow into a microchannel by applying AC voltages to a pair of coplanar meandering electrodes, which can significantly improve the microfluidic mixing. Morin et al. (2007) simulated the AC electroosmosis using an equivalent electric circuit model. They

identified two distinct mechanisms for the AC electroosmosis: the diffusion of ionic species from the bulk to the EDL and the electrochemical reaction on electrode surfaces. More recently, AC electroosmotic flows were adopted to manipulate microtubules in a solution (Uppalapati et al. 2008), which provides a new tool to investigate and control the interactions between microtubules and microtubule motors in vitro. García-Sánchez et al. (2008) experimentally investigated the pumping performance of the traveling wave AC electroosmosis. They found the flow reversal when the voltage is above a threshold, which is attributed to conductivity gradients generated in the bulk liquid due to Faradaic reactions. Ng et al. (2009) reported a novel approach using the AC electroosmosis with DC bias to significantly enhance mixing of two pressure-driven laminar streams flowing in microchannels. This approach provides a new way of breaking the symmetry of the AC electroosmosis by using a DC bias. Chen et al. (2009) presented a comprehensive assessment of micromixing performance for three different AC electroosmotic flow protocols, namely capacitive charging, Faradaic charging and asymmetric polarization. Their results revealed that the Faradaic charging produces much stronger vortices than the other two protocols, and therefore enhances the species mixing. The generation of in-plane microvortices and thus pumping flow in a microchannel was achieved recently with the benefit of AC electroosmotic flow (Huang et al. 2010). The rotational direction of in-plane microvortices and pumping flow direction can be readily controlled by reversing the polarity of applied voltages.

Time-varying AC electric field also can induce a rich variety of colloidal particle assembly around microelectrodes. Under AC electric field, colloidal particles can achieve self-assembly to form two dimensional colloidal crystal near electrodes (Trau et al. 1996, 1997; Yeh et al. 1997). Figure 12 shows the transient formation of two-dimensional colloidal crystal under an AC electric field. This effect was attributed to a rectified electroosmotic flow
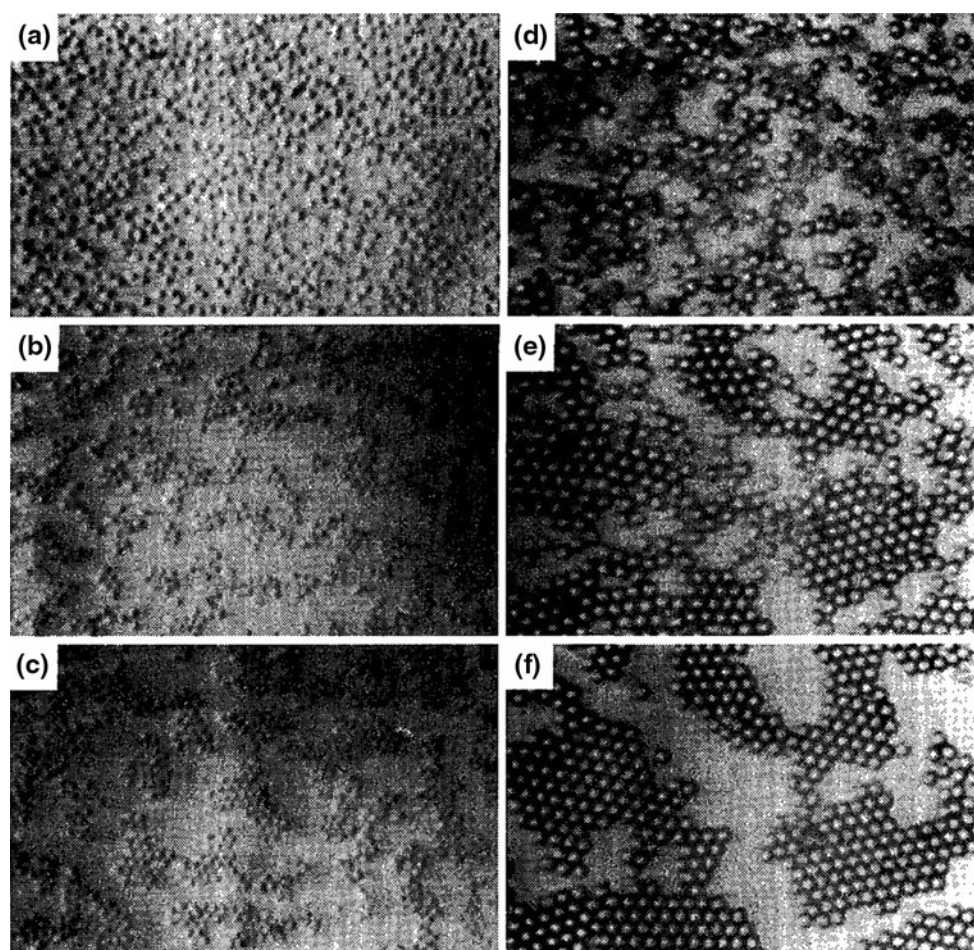
**Fig. 12** Transient formation of two-dimensional colloid crystal over electrode surfaces under an AC electric field. The first column from (**a**) to (**c**) presents the formation process for 900 nm colloidal particles and the second column from (**d**) to (**f**) presents the formation process for 2 μm colloidal particles. The electric field in (**a**) and (**d**) was turned off and the time interval between each frame is 15 s (Trau et al. 1996)

directed radially toward particles, which is resulted from the interaction of an induced inhomogeneous EDL with a non-uniform applied electric field. Later, experiments were conducted to investigate the effects of AC electric field, particle size, and surface charge on the latex particle aggregation on a conducting surface under AC electric fields (Nadal et al. 2002a). It was argued that the competition between electrohydrodynamic attraction and electrostatic dipolar repulsion plays important roles in the particle aggregation. Ristenpart et al. (2003) showed that various patterns of particle assembly can be formed around electrodes when bidisperse colloidal suspensions are under the influence of AC electric fields. Kumar et al. (2005) observed a reversible aggregation of particles in microchannels under AC electric fields. They further demonstrated that such reversible aggregation of particles can be tuned by varying the amplitude and frequency of the applied AC electric field. Since the electrohydrodynamic flow around particles plays important roles in particle

assembly, Ristenpart et al. (2007) performed a detailed analysis for such flows near an electrode with the AC electric forcing. Their analysis ascribed the flow to the thin double layer induced around the particle by AC electric field. Mittal et al. (2008) reported an experiment to measure dipolar forces between micrometer-sized polystyrene latex particles in AC electric fields. They concluded that the dipolar interactions decrease with increasing background salt concentration, which is mainly due to a reduction in the difference between particle and medium conductivities.

The afore-discussed two AC field-driven electrokinetic phenomena, AC electroosmosis and AC particle self-assembly, share some common features. They both occur around electrodes which are actively energized by AC electric field. The two phenomena exhibit strongest when AC frequency takes a particular value, and both phenomena vanish in DC electric fields. In addition, both are proportional to the square of the applied voltage.

Therefore, AC field-driven electrokinetic phenomena can be categorized as non-linear electrokinetic phenomena as compared to the classic linear electrokinetic phenomena in which the resulting fluid or particle velocity is linearly scaled with the applied voltage. Such non-linear dependence can be intuitively understood as follows: The one power of electric field is used to induce charges inside the EDL, and another power of electric field is used to drive these induced charges to generate hydrodynamic flows or particle motion.

### 3.2.2 Induced-charged electrokinetics (ICEK)

Non-linear induced-charge electroosmotic flows are originally observed and discussed in colloid science. Levich (1962) first discussed the induced-charge double layer around a metallic colloidal particle in an external electric field and analyzed the induced flow field around the particle. Since then extensive studies have been carried out by the Ukrainian school for several decades (Dukhin 1986; Dukhin and Murtsovkin 1986; Dukhin and Shilov 1969; Gamayunov et al. 1992; Gamayunov et al. 1986; Murtsovkin 1996; Simonov and Dukhin 1973). Such non-linear flows arise when the applied electric field interacts with the non-electroneutral EDL that is induced by the applied field itself. Recently, several similar non-linear electroosmotic flows driven by both AC and DC electric fields around polarizable objects have draw attention in the microfluidics community. Nadal et al. (2002b) performed a theoretical and experimental study of the microflow patterns produced around a polarizable dielectric stripe deposited on a planar electrode. Their analyses showed that there are two counter-rotating vortices over the dielectric stripe, which is similar to the flow pattern of AC electroosmosis. In a rather different situation, Thamida and Chang (2002) examined a DC-driven non-linear electrokinetic flow around a corner

in a microchannel made of dielectric materials, which can be weakly polarized. Takhistov et al. (2003) experimentally found that non-linear electrokinetic vortices can be induced near microchannel junctions due to the finite polarizability of channel material (as shown in Fig. 13). These examples of non-linear electrokinetic phenomena indicate that polarizable surfaces in microfluidic devices can add new perspectives which do not exist in the conventional linear electrokinetics. The detailed discussion of such type of non-linear electrokinetics can be found in recent reviews by Bazant et al. (2009), Bazant and Squires (2010) and Daghighi and Li (2010).

One should note that electrokinetic phenomena around polarizable surfaces are driven by a same physical mechanism: they all are due to the interaction of the applied field with the charges in EDL induced by the applied field itself, and thus the resulting flow velocity is proportional to the square of applied voltage. To highlight the essential role of induced charges in EDL, the term 'induced-charge electroosmosis' (ICEO) is then suggested for the description of such non-linear electrokinetic flows (Squires and Bazant 2004). Squires and Bazant (2004) also explored its relation to widely studied AC electroosmosis (Ajdari 2000; Ramos et al. 1999). The ICEO generated around asymmetric conducting objects could perform a number of microfluidic applications, such as pumping (Gregersen et al. 2009), mixing (Zhao and Bau 2007), etc. Figure 14 schematically shows the evolution of an external DC electric field around a conducting patch immersed in an electrolyte solution, the formation of induced EDL and the corresponding ICEO above the conducting patch. It is evident that the basic flow pattern of ICEO is a pair of symmetric counter-rotating vortices above the conducting patch. Compared to the well-established and widely used linear electroosmosis associated with non-polarizable surfaces having fixed zeta potentials, ICEO around polarizable surfaces is largely
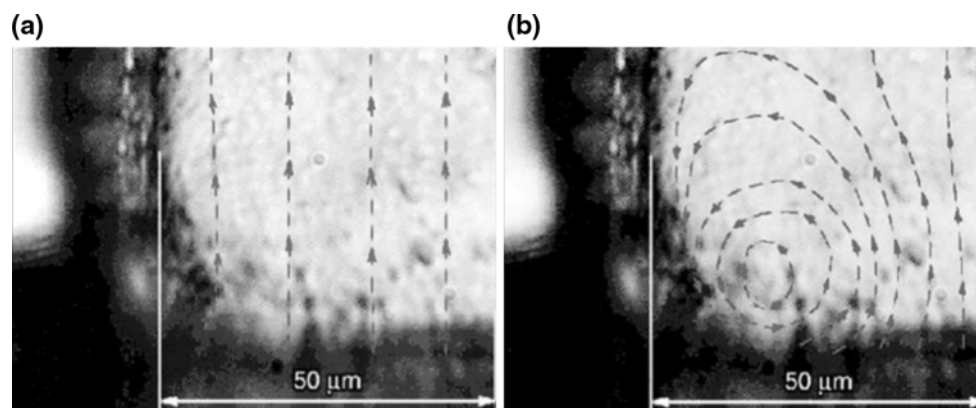


**Fig. 13** The flow patterns at the junction of a microchannel. **a** The sharp corner cannot be polarized by a low electric field strength (20 V/cm) and the irrotational flow pattern of linear electroosmosis is maintained. **b** The sharp corner is polarized by a high electric field strength (50 V/cm) and the irrotational characteristics of linear electroosmotic flow is violated (Takhistov et al. 2003)
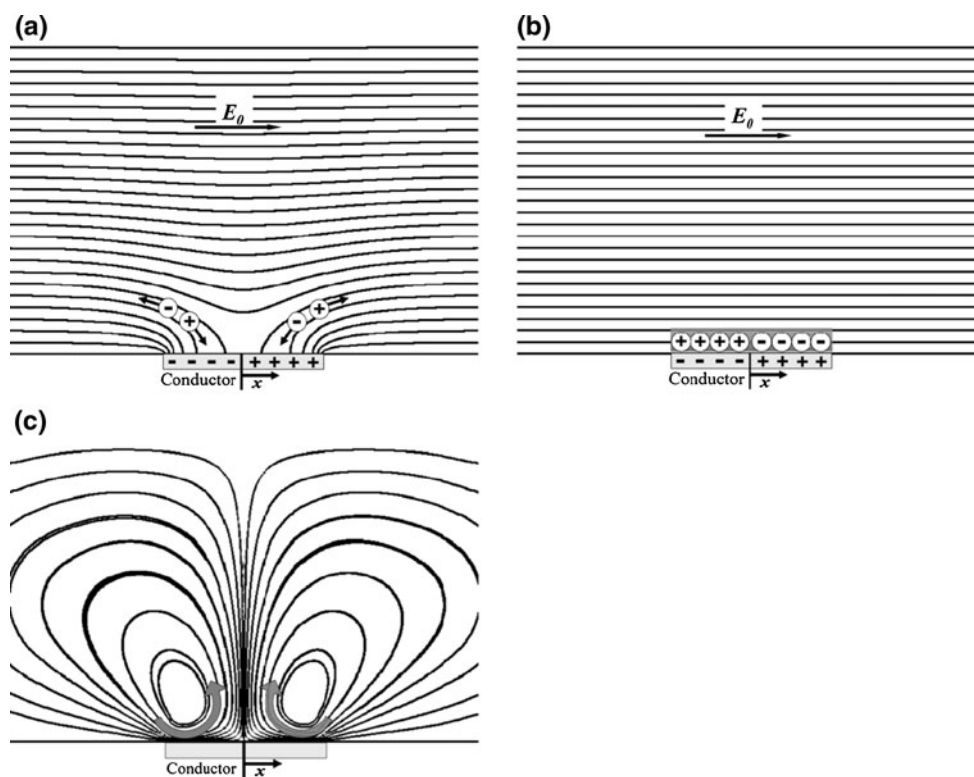
**Fig. 14** Illustration of generation of the induced-charge electroosmosis over a conducting patch. **a** Initially, the conducting patch immersed in an electrolytic solution is subjected to an external DC electric field, and the conducting patch is instantaneously polarized with the electric field lines intersecting the surface at right angles. The right (left) half of the surface acquires positive (negative) charge after polarization. **b** Then such surface charge distribution drives positive ions towards one half of the surface ($x < 0$) and negative ions to the other half ($x > 0$). This process charges up the EDL on the conducting surface. At the steady state, the double layer is fully charged and all the electric field lines become tangential to the surface of conductor. The induced zeta potential is $\zeta_i = -E_0 x$ at the steady state. **c** Finally, the interaction of the external field and the induced double layer causes two nonlinear electroosmotic slip velocities (proportional to the square of $E_0$) directed from both edges toward the center, giving rise to two symmetric vortices above the surface. Since the polarity of the induced charge inside EDL will be reversed by changing the direction of electric field, application of an AC electric field will also produce an identical ICEO flow (Soni et al. 2007)

unnoticed. However, direct control of the shape, position, and potential of conducting or polarizable surfaces in ICEO can introduce numerous interesting and useful effects that do not exist in the conventional linear electroosmosis.

Another aspect of ICEK dubbed induced-charge electrophoresis (ICEP) was also proposed for freely suspended polarizable particles, and can be used for particle manipulations. Although ICEP cannot induce any motion for perfectly spherical particles in uniform electric field, various broken symmetries (such as shape and arrangement asymmetries, non-uniform surface properties and applied fields, anisotropic properties of surrounding liquid) in ICEP can result in particle motion (Kilic and Bazant 2011; Lavrentovich et al. 2010; Squires and Bazant 2006; Wu et al. 2009). Figure 15 presents a simple strategy for inducing the ICEP motion of a conductor with asymmetric shape. The direction of particle motion can be either parallel or perpendicular to the external electric field, depending on shape asymmetry. Another fundamental

discovery of their work is that shape asymmetry can yield quite interesting behaviors, such as the rotation and alignment of the particle with the direction of the electric field. These behaviors however are absent for perfectly spherical particles. The ICEP effect induced by various broken symmetries is possible to transport both charged and uncharged particles as well as conducting and nonconducting particles, thus suggesting potential applications in colloidal manipulation, micromotors, electric display, and microfluidic devices.

Zeta potential is a very important parameter in electrokinetics. Theoretical characterization of induced-charge electrokinetics needs efficient evaluation of the induced zeta potentials of polarizable surfaces. Most existing studies reported induced-charge electrokinetics of ideally polarizable surfaces (i.e., conductors with good conductivities), but less attention has been paid to more general situations involving finitely polarizable or semiconducting surfaces. Zhao (2012) derived a generalized electric

**Fig. 15** Translocation of an asymmetric conductor with zero net charge in horizontally and vertically applied uniform electric fields. The upper row denotes the ICEP induced motion due to broken fore-aft symmetry of the conductor, and the conductor moves by ICEP towards its wide end side. The direction of the ICEP motion is opposite to the direction of the applied electric field. **a** Electric field lines and **b** streamlines of the ICEO flow for the broken fore-aft symmetry. The *lower row* denotes the ICEP induced motion due to broken left–right symmetry of the conductor, and the conductor moves by ICEP towards its narrow end side. The direction of the ICEP motion is perpendicular to the direction of the electric field (**c**) Electric field lines and (**d**) streamlines of the ICEO flow for the broken left–right symmetry (Squires and Bazant 2006)
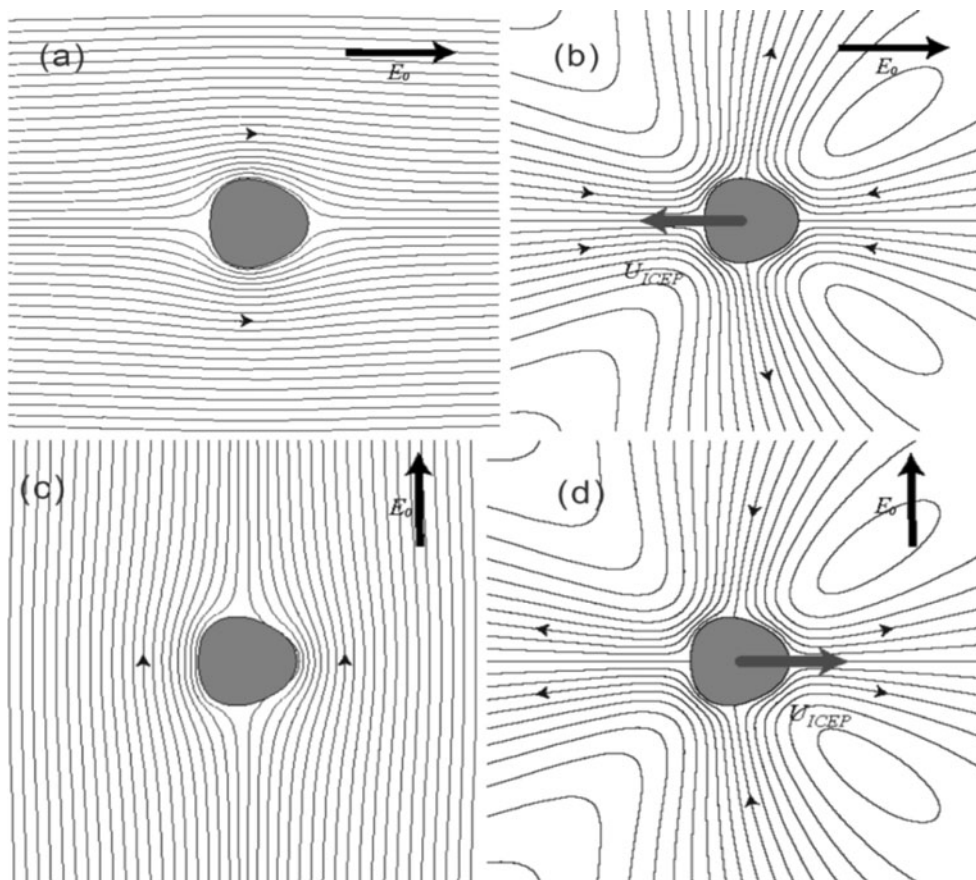
boundary condition describing induced-charge phenomena over arbitrarily polarizable dielectric surfaces. Such boundary condition connects the potentials in the dielectric domain and the bulk fluid domain as shown in Fig. 16, and is expressed as (Zhao 2012)
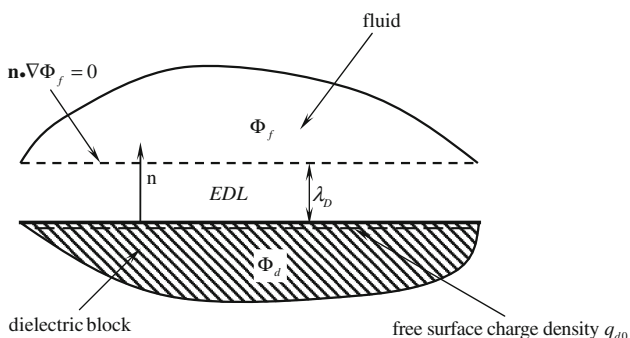


**Fig. 16** Schematic illustration of an electric boundary condition for induced-charge electrokinetic phenomena at the interface between an electrolyte fluid and a polarizable dielectric object. The potential in the bulk fluid $\Phi_f$ and the potential in the dielectric block $\Phi_d$ both satisfy the Poisson equation. The induced zeta potential can be determined as the difference between the potential on surface of the dielectric block and the potential at the outer edge of EDL, i.e., $\Phi_d|_{n=0} - \Phi_f|_{n=\lambda_D}$ (Zhao and Yang 2009)

$$\lambda_D \frac{\varepsilon_d}{\varepsilon_f} \mathbf{n} \cdot \nabla\Phi_d\bigg|_{n=o} = 2\frac{K_B T}{ze}\sinh\left[\frac{ze(\Phi_f|_{n=\lambda_D} - \Phi_d|_{n=0})}{2K_B T}\right] + \zeta_{d0} \tag{17}$$

where $\varepsilon_d$ and $\varepsilon_f$ are dielectric constants of dielectric block and electrolyte fluid, respectively, and $\zeta_{d0}$ is the conventional zeta potential corresponding to natural surface charge density $q_{d0}$ and is related to $q_{d0}$ by (Squires and Bazant 2004)

$$\zeta_{d0} = \frac{\lambda_D q_{d0}}{\varepsilon_0 \varepsilon_f} \tag{18}$$

Due to the non-linear hyperbolic sine function involved in Eq. (17), numerical methods are needed to solve the equation for obtaining the induced zeta potential. However, when the potential drop across the EDL is small, Eq. (17) is reduced to a linearized boundary condition of Robin type expressed as

$$\Phi_d|_{n=0} + \lambda_D\frac{\varepsilon_d}{\varepsilon_f} n \cdot \nabla\Phi_d\bigg|_{n=0} = \Phi_f|_{n=\lambda_D} + \zeta_{d0} \tag{19}$$

Equation (19) exactly recovers the result of Yossifon et al. (2006) and Yossifon et al. (2007) who obtained the same boundary condition for small induced zeta potentials

by using the asymptotic matching. The advantage of this boundary condition lies in its linearity which facilitates evaluation of the induced zeta potential analytically. In addition to the steady state situation, transient version of these boundary conditions also has been derived by Yossifon et al. (2009).

Furthermore from a more general viewpoint, a solid can have both finite dielectric constant and conductivity, and is leaky dielectric or semiconductive in nature. Under these circumstances, free charge carriers are present not only in the liquid but also inside the solid. Consequently, the space charge layer (SCL) is formed in the solid (Bardeen 1947; Bockris and Reddy 2004; Bockris et al. 2002; King and Freund 1984), in a similar fashion to the EDL formed in the electrolyte liquid under the influence of external electric fields. These two EDL and SCL layers constitute the interface between a semiconductor and an electrolyte solution. Other than the induced surface charge due to polarization, free charge stored in the SCL because of electric conduction also contributes to the induced zeta potential. Zhao and Yang (Zhao and Yang 2011a, b) presented electrokinetic boundary conditions for AC field-driven ICEK to correlate the bulk electrical potentials across the EDL and the SCL at a semiconductor-electrolyte solution interface. As the interface between an electrolyte fluid and a semiconductor shown in Fig. 17 is concerned, generalized electrokinetic boundary conditions for an AC electric field with arbitrary wave forms can be obtained as (Zhao and Yang 2011a)
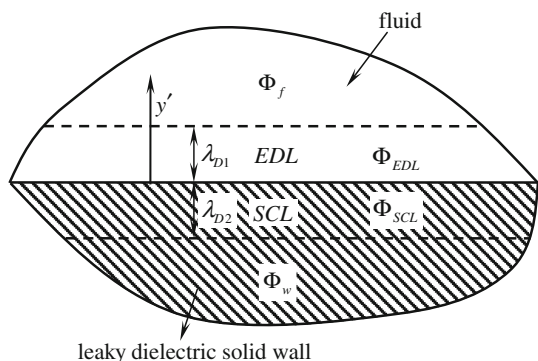


**Fig. 17** Schematic representation of the interface between an electrolyte fluid and a semiconductor. Electrostatic problem near the interface can be divided into four sub-domains, namely, (i) the bulk electrolyte fluid domain $\Phi_f$, (ii) the bulk leaky dielectric solid wall domain $\Phi_w$, (iii) the EDL domain $\Phi_{EDL}$ inside the liquid and (iv) the SCL domain $\Phi_{SCL}$ inside the solid. The dash lines inside the electrolyte fluid and solid wall respectively represent the outer edges of the EDL and SCL where $\Phi_{EDL}$ matches $\Phi_f$ and $\Phi_{SCL}$ matches $\Phi_w$. $\lambda_{D1}$ and $\lambda_{D2}$ denote the thicknesses of EDL and SCL, respectively (Zhao and Yang 2011a)

$$\Phi_f^{(k)} - \Phi_w^{(k)} = \frac{d\Phi_f^{(k)}}{dy} \frac{\delta_1}{\gamma_1(\gamma_1^2 - 1)} + \frac{d\Phi_w^{(k)}}{dy} \frac{\delta_2}{\gamma_2(\gamma_2^2 - 1)}$$
$$\text{at } y = 0 \qquad (20)$$

$$\delta_1 \frac{\gamma_1^2}{(\gamma_1^2 - 1)} \frac{d\Phi_f^{(k)}}{dy} - \beta\delta_2 \frac{\gamma_2^2}{(\gamma_2^2 - 1)} \frac{d\Phi_w^{(k)}}{dy} = 0 \quad \text{at } y = 0$$
$$\qquad (21)$$

where $y = y'/a$, $\delta_1 = \lambda_{D1}/a$, $\delta_2 = \lambda_{D2}/a$, $\gamma_1^2 = 1 + jk\Omega$ ($j = \sqrt{-1}$), $\gamma_2^2 = 1 + t_w jk\Omega/t_f$, $\beta = (\varepsilon_w\lambda_{D1})/(\varepsilon_f\lambda_{D2})$ with $t_f = \lambda_{D1}^2/D_f$ and $t_w = \lambda_{D2}^2/D_w$. In above equations, superscript $k$ denotes the $k$th term of Fourier series expansion for electric potential, $a$ represents the characteristic dimension of the semiconducting solid, $\Omega$ is the normalized AC frequency with respect to the Debye frequency $\omega_D$ of electrolyte solution ($\omega_D = 1/t_f$). $\varepsilon_w$ and $\varepsilon_f$ are dielectric constants of semiconducting solid and electrolyte fluid, respectively. $D_w$ and $D_f$ are diffusion coefficients of charge carriers in semiconducting solid and electrolyte fluid, respectively. Such general electrokinetic boundary conditions are applicable to the AC field-driven induced-charge electrokinetics over solids of any dielectric constants and conductivities under electric field with arbitrary wave forms. For given values of $\beta$ and $t_w/t_f$, the solution of the electrostatic problem requires the simultaneous determination of bulk potentials, $\Phi_f^{(k)}(\mathbf{r})$ and $\Phi_w^{(k)}(\mathbf{r})$ (where $\mathbf{r}$ denotes the position vector), which are harmonic (governed by Laplace's equation) within the respective bulk fluid and bulk solid domains, and satisfy the boundary conditions Eqs. (20) and (21) on the surface of semiconducting solids as well as the far-field conditions for $\Phi_f^{(k)}(r)$. After solving electrostatic problem, one can determine the induced zeta potential as $-\delta_1\left(d\Phi_f^{(k)}/dy\big|_{y=0}\right)/\left[\gamma_1(\gamma_1^2 - 1)\right]$.

Equations (20) and (21) physically describe the charging of SCL and EDL at an electrolyte-semiconductor interface. The first term on the right-hand side of Eq. (20) denotes the potential drop across EDL (so-called induced zeta potential), while the second term denotes the potential drop across the SCL. After rearranging the charging equation for EDL, one can obtain (Zhao 2012)

$$\frac{d\Phi_f^{(k)}}{dy} = -\zeta_i^{(k)} jk\omega \frac{\lambda_{D1}a}{D_f} \sqrt{1 + jk\frac{\omega}{\omega_D}} \quad \text{at } y = 0 \qquad (22)$$

from which one can identify the time scale for the charging of EDL is $\lambda_{D1}a/D_f$ when the frequency of external electric field ($\omega$ in dimensional form) is much less than the Debye frequency $\omega_D$. This time scale ($\lambda_{D1}a/D_f$) is of critical importance for characterizing AC field-induced charge electrokinetics. It should be noted from Eqs. (20) and (21) that for a semiconductor-electrolyte interface two time

scales ($\lambda_{D1}a/D_f$ for the charging of EDL and $\lambda_{D2}a/D_w$ for the charging of SCL) compete under the AC electric field. When $\lambda_{D1}a/D_f$ is much smaller than $\lambda_{D2}a/D_w$, the potential drop across the interface is mainly on the liquid electrolyte side, while when $\lambda_{D1}a/D_f$ is much larger than $\lambda_{D2}a/D_w$, the potential drop across the interface is mainly on the solid semiconductor side. At last, one should note that the above effective electrokinetic boundary conditions involve two assumptions, i.e., low applied voltages and thin EDLs. For large voltages and thick EDLs, effects of surface conduction (Bazant et al. 2004; Chu and Bazant 2006) and ion size (Højgaard Olesen et al. 2010; Kilic et al. 2007; Storey et al. 2008) become pronounced, and thus modifications for these electrokinetic boundary conditions are required to take into account such effects.

Attention also has been paid to explore ICEK phenomena for microfluidic applications. Levitan et al. (2005) experimentally demonstrated the ICEO around a platinum wire immersed in a KCl solution under an AC electric field. It was shown that the ICEO driven by weak AC electric field exhibits more general frequency dependence in comparison with the ACEO, even allowing for a steady flow under a DC electric field. Bazant and Ben (2006) presented new guidelines for designing high-flow rate 3D AC electroosmotic pumps based on the concept of ICEO, and the creation of ICEO flow conveyor belt over a stepped electrode array was identified to be the most effective pumping configuration. Leinweber et al. (2006) utilized the ICEK to realize a continuous demixing process in a microfluidic device. The process relies on noble metal posts floating in high external electrical field. It was shown that such microfluidic demixer can achieve the efficient demixing of a homogeneous electrolyte into concentrated laminae and depleted laminae. Using ICEO microvortices produced by an AC field, Harnett et al. (2008) reported a microfluidic mixer for microfluidic sample preparation. In addition, they showed the mixer can also prevent sample dilution and thus maintain detection sensitivity. Wu and Li (2008) patterned PDMS microchannels with platinum-conducting surfaces for generation of ICEO, this strategy was demonstrated both experimentally and numerically for mixing enhancement. More recently, the localized control of pressure driven flow near conductive surfaces was presented with the use of ICEO (Sharp et al. 2011). It was shown that the ICEO flows introduced by conducting structures enable an on/off switch of fluid flow in a microfluidic device.

The idea of induced-charge electrokinetics is also extended for particle manipulations. Yariv (2005) theoretically analyzed the ICEP motion of non-spherical conducting particles. It was demonstrated that unlike the conventional linear electrophoresis, non-spherical particles with zero net charge can translate and/or rotate in response

to the applied electric field because of the ICEP. Saintillan et al. (2006) examined the hydrodynamic interaction in the ICEP of infinitely polarizable slender rods. In particular, they showed that the non-linear ICEO flow on the particle surfaces causes alignment of the rods in the direction of the electric field and induces linear distributions of point-force singularities. Then the stresslet disturbance flows are induced by such distribution of point forces to produce hydrodynamic interactions between the rods. The experimental verifications of these ICEO and ICEP effects were demonstrated by (Rose et al. 2007). Gangwal et al. (2008) presented a study of the motion of Janus microparticles with one dielectric and one metal-coated hemisphere due to ICEP. It was found that the direction of Janus particle motion is perpendicular to the external driving field, which differs from the conventional linear electrophoresis. Miloh (2008) gave a systematic analysis of the motion of conducting particles with arbitrary shape under both DC and AC non-uniform electric fields. It was highlighted that the dipolophoresis (combination of dielectrophoresis and ICEP) is the driving mechanism for particle motion. More recently, Daghighi et al. (2011) constructed a 3D numerical model to investigate the motion of Janus particles in microchannels via ICEP. This study reveals that ICEO vortices produced on the polarizable side of the Janus particle push the Janus particle to move faster than the non-polarizable and entirely polarizable particles (see Fig. 18). The direction of the Janus particle motion can be tuned by adjusting the orientation of the polarizable part of Janus particles.

Finally, we would like to point out the differences between induced-charge electrokinetic phenomena and AC field-driven electrokinetic phenomena reviewed in previous sections. The AC field-driven electrokinetic phenomena occur around conducting electrodes with actively applied voltages, and the induced-charge electrokinetic phenomena occur around polarizable materials (not necessarily conducting) floating in external electric fields. The AC field-driven electrokinetic phenomena disappear at the DC limit, while the induced-charge electrokinetic phenomena in principle should be the strongest at the DC limit. In addition, it seems that both theories and applications of induced-charge electrokinetic phenomena are only limited to microfluidics at the present stage, and the extension of induced-charge electrokinetics to nanofluidics could be promising.

### 3.2.3 Second-kind electrokinetics

Second-kind electrokinetic flows usually occur around conducting porous materials under the effects of large applied electric field. Under a large electric field, strong concentration polarization and space charges are produced
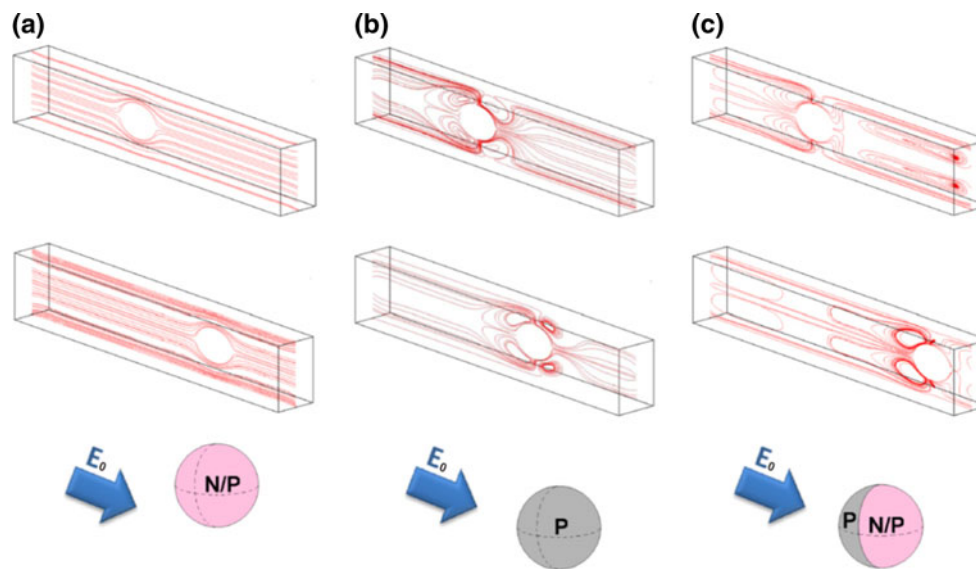
**Fig. 18** Comparison among the electrophoretic motion of three different types of particles in a microchannel. **a** A non-polarizable particle with a natural zeta potential of 60 mV, **b** an entirely polarizable particle with zero net charge, **c** a Janus particle. "*P*" represents "polarizable" and "*N/P*" represents "non-polarizable". For all cases the zeta potential on the microchannel wall and the external electric field are set to be the same. The *top row* shows the initial locations of particles in microchannels, the *middle row* shows particle locations after a same period of time. The *bottom row* shows the orientation of the particles with respect to the external field (Daghighi et al. 2011)

in the bulk electrolyte due to strong current of certain ions through the conducting surface. Then the fluid motion due to electrokinetics of the second kind is triggered by the interaction of the space charges with the applied field (Dukhin 1991). This mechanism also not only can explain the similar phenomena which occur near non-porous conducting surfaces with very strong electrochemical reactions (Barany et al. 1998), but also the catalytically induced electrokinetics (Kline et al. 2005; Moran and Posner 2011; Paxton et al. 2006); for the latter the driving electric field however is not externally applied, instead it is induced by the electrochemical reactions around a Janus particle with two dissimilar metal segments.

A classical picture of the second-kind electrokinetic flow is depicted by Dukhin's model which characterizes an "electroosmotic whirlwind" around a highly conductive spherical particle subject to a strong electric field and a corresponding bulk charge layer induced in the electrolyte solution, as shown in Fig. 19. This effect could be incorporated in electrochromatographic systems to greatly facilitate rapid separations (Rathore and Horvath 1997). Second-kind electrokinetics and space charge formation also can occur in systems with microchannel-nanochannel junctions, as illustrated in Fig. 20. In a nanochannel with EDL overlapping, counterions predominate over co-ions to neutralize the charge on nanochannel walls. Under an external electric field, the nanochannel mainly conducts a current of counterions, which can be strong enough to deplete the bulk salt concentration in the microchannel. At
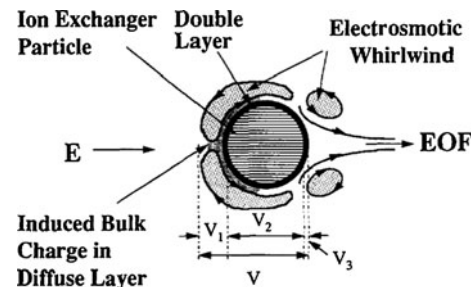


**Fig. 19** Schematic illustration of Dukhin's model in which an induced bulk charge layer and electroosmotic whirlwind form around a highly conductive ion-exchange particle subject to a high electric field. *V* is the total potential drop across the entire domain, and it is composed of $V_1$ (potential drop across the bulk charge layer), $V_2$ (potential drop across the particle itself), and $V_3$ (potential drop across the EDL) (Rathore and Horvath 1997)

the steady state, a space charge layer of counterions is induced near the microchannel-nanochannel junction. The second-kind electrokinetic flows thus occur because of the interaction of the tangential electric field near the junction with the space charge layer surrounding the junction.

Mishchuk et al. (2001) analyzed both theoretically and experimentally the phenomena of limiting current and strong concentration polarization around flat and curved interfaces. They found out that the current through the curved interface grows rapidly, while the current tends to saturate for the case of the flat surface. This is mainly due to an important change of characteristics of concentration
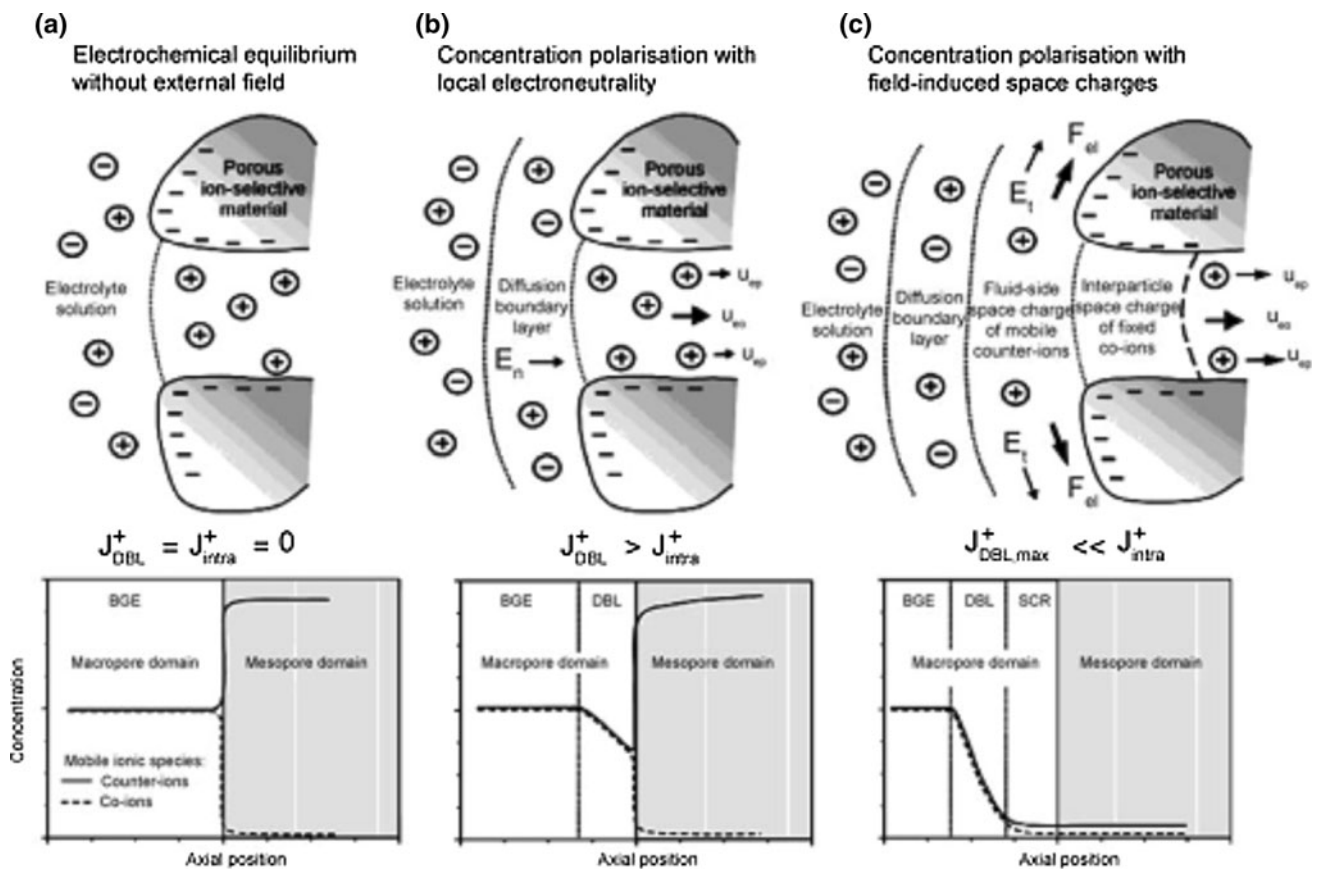
**Fig. 20** Schematic illustration of the mechanism for the formation of space charge and second-kind electroosmosis at the microchannel-nanochannel junction. **a** In the absence of external electric field, the microchannel contains neutral electrolyte and the nanochannel mainly contains counterions due to the overlapping of EDLs. **b** With an applied electric field, the counterions are mainly conducted through the nanochannel. Then the nearby salt concentration in the micro-channel is depleted, which introduces a bulk diffusion layer. **c** The bulk concentration can be depleted completely under a strong electric field, which leads to the formation of space charge layer and thus second-kind electroosmosis around the microchannel-nanochannel junction (Leinweber and Tallarek 2004)

polarization generated by electroosmosis of the second kind near the curved interface. Ben and Chang (2002) theoretically predicted the generation of microvortices around an ion-exchange porous granule and attributed it to electrokinetic phenomena of the second kind. Based on electroosmosis of the second kind, a low-voltage micropump was developed (Heldal et al. 2007). This kind of micropumps offers several advantages: no moving parts, small power/voltage and dimensions, situated inside the flow channel. These advantages make the pumps suitable for portable, embedded and implantable microfluidic devices. Micropumps utilizing electroosmosis of the second kind were also successfully tested using AC electric field (Mishchuk et al. 2009), in good agreement with the theoretical predictions. The AC field eliminates the possibility of bubble generation in the operation of microfluidic and lab-on-a-chip systems. More recently, Kivanc and Litster (2011) presented a micropump made of mesoporous silica skeletons and driven by electroosmosis of the second kind. Other than fluid motion, second-kind electrokinetics

also can induce particle motion. Dukhin et al. (1989) established the existence of electrophoresis of the second kind for metallic particles. Barany et al. (1998) demonstrated that electrophoretic velocities of the conducting particles are much higher than those expected for non-conducting particles. They attributed this scenario to electrokinetics of the second kind. Usually, a bulk charge layer is induced outside the primary EDL when the externally applied electric is high enough to produce the over limit current through the particle. This extra-induced bulk charge layer in turn interacts with the external electric field, leading to the enhancement of electrophoretic motion. In an independent work by (Ben et al. 2004), the above reasoning for electrophoretic velocity enhancement due to electrophoresis of the second kind was corroborated.

However, second-kind electrokinetics requires large applied electric field and thus triggers strong surface and bulk chemical reactions, which are usually unwanted in most biomedical-related microfluidic applications. Furthermore, one should note that there are distinct differences between

the ICEK and the second-kind electrokinetics. Second-kind electrokinetic phenomena are driven by space charges in the bulk solution, but not in the EDL. In contrast, ICEK relies on relatively small charges in the EDL-induced around polarizable surfaces, rather than bulk space charges. In particular, ICEK does not induce Faradaic reactions because of relatively low driving voltages, which thus makes the ICEK a suitable candidate for biomedical applications.

We close the review by noting that there are still new electrokinetic techniques being developed. One recent example is the electrically induced locomotion of a conducting particle due to asymmetric bubbles generated by electrochemical reactions (oxidation and reduction) on two hemispheres of the particle (Loget and Kuhn 2010, 2011). In this technique, the velocity of particle motion can be controlled by modulation of asymmetric bubble generation, as shown in Fig. 21, and the method is shown effective for particles with sizes ranging from microns to centimeters. This electrokinetic technique cannot be classified into any subcategory reviewed above because of new physical

mechanisms involved, thereby indicating the great versatility of the family of electrokinetic phenomena.

## 4 Conclusions and suggestions for future investigation

Electrokinetic phenomena can occur over both insulating (non-polarizable) and polarizable (conducting) surfaces. Electrokinetics involving insulating surfaces induces particle or fluid velocity, which is linearly proportional to the strength of external electric field, and known as the linear electrokinetics. While electrokinetics involving conducting or polarizable surfaces induces particle or fluid velocity which is linearly proportional to the square of external electric field strength, and thus known as non-linear electrokinetics. In comparison with linear electrokinetics, non-linear electrokinetic phenomena are new to the family of electrokinetics. In addition, the non-linear relationship with applied electric fields enables electrokinetics to generate not only much larger flow rates for liquids or velocities for
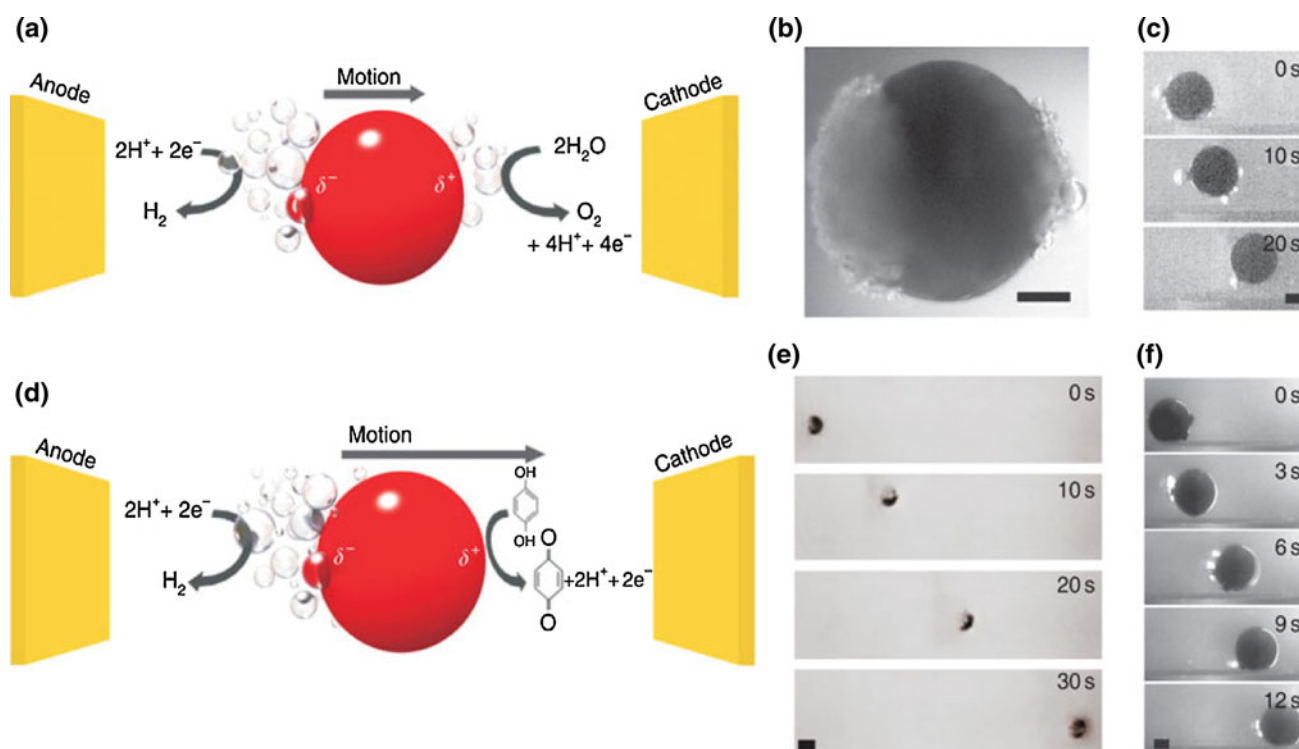


**Fig. 21** Locomotion of spherical conducting objects due to asymmetric bubble generation induced by electrochemical reactions. The *upper row* (**a**–**c**) shows the unequal bubble production at two hemispheres. **a** Water splitting by bipolar electrochemical reactions. **b** Microscopic image of a 1 mm stainless steel particle in the $H_2SO_4$ aqueous solution under the influence of an electric field. $H_2$ bubbles are produced on the left hemisphere facing the anode and $O_2$ bubbles are produced on the hemisphere facing the cathode. *Scale bar*, 250 μm. **c** Translational motion of a 285 μm glassy carbon sphere driven by an electric field in a PDMS microchannel filled with the $H_2SO_4$ aqueous solution. *Scale bar*, 100 μm. The *lower row* (**d**–**f**) shows the elimination of $O_2$ bubble production. **d** Elimination of $O_2$ bubbles due to hydroquinone oxidation. **e** Translational motion of a 1 mm stainless steel bead in an aqueous solution of HCl and hydroquinone under an electric field. *Scale bar*, 1 mm. **f** Translational motion of a 275 μm glassy carbon sphere driven by an electric field in a PDMS microchannel filled with an aqueous solution of HCl and hydroquinone. *Scale bar*, 100 μm (Loget and Kuhn 2011)

particles but also net motion of liquids and particles under zero-mean AC driving electric fields.

Electrokinetic phenomena with surface charge patterning, electrokinetic phenomena with active surface charge modulation and electrokinetic phenomena with hydrophobic surfaces are reviewed under the category of linear electrokinetics. In these three subcategories, the first two are well understood and their applications in micro- and nano-fluidics are diverse. However, the third one just emerges from the literature and most of investigations are purely theoretical. With current state-of-the-art micro- and nano-fabrications techniques, hydrophobic or superhydrophobic surfaces are readily available (Shiu et al. 2004; Wang et al. 2006; Zhang et al. 2005). Then experimental investigations are highly necessary to verify existing theoretical predictions of electroosmotic flow over superhydrophobic surfaces. Furthermore, superhydrophobic surfaces also can be readily engineered to achieve desired patterns of both hydrodynamic slip and surface charge, thereby promising a large number of electrokinetic effects that could be used for micro- and nano-fluidic applications.

AC electric field driven electrokinetics, induced-charge electrokinetics and electrokinetics of the second kind are reviewed under the category of non-linear electrokinetics. In AC field driven electrokinetics, electrodes are powered to supply driving electric field. Then complicated electrode designs are indispensable for highly integrated microfluidic systems. Due to inherent surface and bulk chemical reactions, electrokinetics of the second kind is not suitable for microfluidics, which frequently handles biosamples. In comparison with the above two types of non-linear electrokinetics, induced-charge electrokinetics, however, utilizes electrically polarizable surfaces floating in a global driving electric field. This global driving field can be simply set up by two electrodes, which thus requires a much simpler electrode design. Moreover, induced-charge electrokinetics relies on the double layer charges induced by low voltages and thus does not suffer from surface and bulk electrochemical reactions.

As a result, induced-charge non-linear electrokinetics merits further investigation in micro- and nanofluidics. At the present stage, the applications of induced-charge electrokinetics are very limited as compared to other two non-linear electrokinetic phenomena. To our best knowledge, only few microfluidic applications for induced-charge electrokinetics have been reported, such as microfluidic mixing and particle transportation. Thus, the applications of induced-charge electrokinetics in microfluidics need to be further expanded. On the other hand, nanofluidics, an extension of microfluidics to nanometer scale, mainly involves manipulations of charged molecules and ions in nanochannels. Because of overlapping EDLs, transport of charged species in nanochannels is dominated by the surface charge density on the walls of nanochannels. Then active control of nanofluidic systems requires the direct modulation of surface charges on the nanochannel walls. It is clear that induced-charge electrokinetics is a natural choice for such purpose, because the surface charge density can be actively controlled by altering the strength of external electric field or the surface orientation with respect to the external electric field. Consequently, the extension of induced-charge electrokinetics from microfluidics to nanofluidics is necessary. To integrate induced-charge electrokinetic effects into nanofluidic systems for controlling charged species transport, nanochannels with conducting walls are needed. The recently established techniques allow for manufacturing such nanochannels. Nanochannels with dimensions ranging from several nanometers to several tens of nanometers can be fabricated on silicon substrates by using reactive ion etching or wet etching (Duan and Majumdar 2010; Mao and Han 2005; Park et al. 2009), and then the nanochannel walls can be made conductive by coating them with thin conducting films (such as gold or platinum) by using the standard sputtering process or electron beam evaporation process.

Electrokinetics literally means the motion induced by electricity. Consequently, other than EDL-related electrokinetic phenomena mentioned in this review, lots of other related effects, such as dielectrophoresis, electrowetting, electrospray and so on (not included in this review), all actually can be classified as electrokinetics. This suggests great versatility of electrokinetic phenomena. Because of such versatility and the readily available electricity, it is certainly expected that there are still new electrokinetic techniques being or to be developed for many years to come.

## References

Ajdari A (1995) Electro-osmosis on inhomogeneously charged surfaces. Phys Rev Lett 75:755–758

Ajdari A (2000) Pumping liquids using asymmetric electrode arrays. Phys Rev E 61:R45–R48

Ajdari A (2001) Transverse electrokinetic and microfluidic effects in micropatterned channels: Lubrication analysis for slab geometries. Phys Rev E 65:016301

Ajdari A, Bocquet L (2006) Giant amplification of interfacially driven transport by hydrodynamic slip: diffusio-osmosis and beyond. Phys Rev Lett 96:186102

Anderson JL (1985) Effect of nonuniform zeta potential on particle movement in electric fields. J Colloid Interface Sci 105:45–54

Anderson JL (1989) Colloid Transport by Interfacial Forces. Annu Rev Fluid Mech 21:61–99

Anderson JL, Idol WK (1985) Electroosmosis through pores with nonuniformly charged walls. Chem Eng Commun 38:93–106

Bahga SS, Vinogradova OI, Bazant MZ (2010) Anisotropic electro-osmotic flow over super-hydrophobic surfaces. J Fluid Mech 644:245–255

Barany S, Mishchuk NA, Prieve DC (1998) Superfast electrophoresis of conducting dispersed particles. J Colloid Interface Sci 207:240–250

Bardeen J (1947) Surface states and rectification at a metal semi-conductor contact. Phys Rev 71:717–727

Barrat JL, Bocquet L (1999a) Influence of wetting properties on hydrodynamic boundary conditions at a fluid/solid interface. Faraday Discuss 112:119–128

Barrat JL, Bocquet L (1999b) Large slip effect at a nonwetting fluid-solid interface. Phys Rev Lett 82:4671–4674

Bazant MZ, Ben Y (2006) Theoretical prediction of fast 3D AC electro-osmotic pumps. Lab Chip 6:1455–1461

Bazant MZ, Squires TM (2004) Induced-charge electrokinetic phenomena: theory and microfluidic applications. Phys Rev Lett 92:066101

Bazant MZ, Squires TM (2010) Induced-charge electrokinetic phenomena. Curr Opin Colloid Interface Sci 15:203–213

Bazant MZ, Thornton K, Ajdari A (2004) Diffuse-charge dynamics in electrochemical systems. Phys Rev E 70:021506

Bazant MZ, Kilic MS, Storey BD, Ajdari A (2009) Towards an understanding of induced-charge electrokinetics at large applied voltages in concentrated solutions. Adv Colloid Interface Sci 152:48–88

Belyaev AV, Vinogradova OI (2011) Electro-osmosis on anisotropic superhydrophobic surfaces. Phys Rev Lett 107:098301

Ben Y, Chang HC (2002) Nonlinear smoluchowski slip velocity and micro-vortex generation. J Fluid Mech 461:229–238

Ben Y, Demekhin EA, Chang HC (2004) Nonlinear electrokinet-ics and "superfast" electrophoresis. J Colloid Interface Sci 276:483–497

Bockris JOM, Reddy AKN (2004) Modern electrochemistry 2B: electrodics in chemistry, engineering, biology, and environmen-tal science. Kluwer Academic Publishers, New York

Bockris JOM, Reddy AKN, Gamboa-Aldeco ME (2002) Modern electrochemistry 2A: fundamentals of electrodics. Kluwer Academic Publishers, New York

Bocquet L, Barrat J-L (2007) Flow boundary conditions from nano- to micro-scales. Soft Matter 3:685–693

Brotherton CM, Davis RH (2004) Electroosmotic flow in channels with step changes in zeta potential and cross section. J Colloid Interface Sci 270:242–246

Chen JK, Weng CN, Yang RJ (2009) Assessment of three AC electroosmotic flow protocols for mixing in microfluidic chan-nel. Lab Chip 9:1267–1273

Cheng L-J, Guo LJ (2010) Nanofluidic diodes. Chem Soc Rev 39:923–938

Chiara N, Drew RE, Elmar B, Hans-Jürgen B, Vincent SJC (2005) Boundary slip in Newtonian liquids: a review of experimental studies. Rep Prog Phys 68:2859

Chu KT, Bazant MZ (2006) Nonlinear electrochemical relaxation around conductors. Phys Rev E 74:011501

Constantin D, Siwy ZS (2007) Poisson-Nernst-Planck model of ion current rectification through a nanofluidic diode. Phys Rev E 76:041202

Cottin-Bizonne C, Cross B, Steinberger A, Charlaix E (2005) Boundary slip on smooth hydrophobic surfaces: intrinsic effects and possible artifacts. Phys Rev Lett 94:056102

Craig VSJ, Neto C, Williams DRM (2001) Shear-dependent boundary slip in an aqueous Newtonian liquid. Phys Rev Lett 87:054504

Daghighi Y, Li D (2010) Induced-charge electrokinetic phenomena. Microfluid Nanofluid 9:593–611

Daghighi Y, Gao Y, Li D (2011) 3D numerical study of induced-charge electrokinetic motion of heterogeneous particle in a microchannel. Electrochim Acta 56:4254–4262

Daiguji H, Yang P, Majumdar A (2003) Ion transport in nanofluidic channels. Nano Lett 4:137–142

Daiguji H, Oka Y, Shirono K (2005) Nanofluidic diode and bipolar transistor. Nano Lett 5:2274–2280

Davidson C, Xuan X (2008) Electrokinetic energy conversion in slip nanochannels. J Power Sources 179:297–300

Delgado ÁV, Arroyo FJ (2002) Electrokinetic phenomena and their experimental determination: an overview. In: Delgado ÁV (ed) Interfacial electrokinetics and electrophoresis. Marcel Dekker, New York

Delgado AV, González-Caballero F, Hunter RJ, Koopal LK, Lyklema J (2007) Measurement and interpretation of electrokinetic phenomena. J Colloid Interface Sci 309:194–224

Duan C, Majumdar A (2010) Anomalous ion transport in 2-nm hydrophilic nanochannels. Nat Nanotechnol 5:848–852

Dukhin AS (1986) Pair interaction of disperse particles in electric field. 3. Hydrodynamic interaction of ideally polarizable metal particles and dead biological cells. Colloid J USSR 48:376–381

Dukhin SS (1991) Electrokinetic phenomena of the second kind and their applications. Adv Colloid Interface Sci 35:173–196

Dukhin SS (1993) Non-equilibrium electric surface phenomena. Adv Colloid Interface Sci 44:1–134

Dukhin AS, Murtsovkin VA (1986) Pair interaction of particles in electric field. 2. influence of polarization of double layer of dielectric particles on their hydrodynamic interaction in a stationary electric field. Colloid J USSR 48:203–209

Dukhin SS, Shilov VN (1969) Theory of the static polarization of the diffuse part of the thin double layer of spherical particles. Colloid J USSR 31:564–570

Dukhin SS, Tarovskii AA, Baran AA (1989) Electrophoresis of the second kind for metallic particles. Colloid J USSR 50:1058–1059

Eijkel J (2007) Liquid slip in micro- and nanofluidics: recent research and its possible implications. Lab Chip 7:299–301

Fan R, Yue M, Karnik R, Majumdar A, Yang P (2005) Polarity switching and transient responses in single nanotube nanofluidic transistors. Phys Rev Lett 95:086607

Fan R, Huh S, Yan R, Arnold J, Yang P (2008) Gated proton transport in aligned mesoporous silica films. Nat Mater 7:303–307

Gamayunov NI, Murtsovkin VA, Dukhin AS (1986) Pair interaction of particles in electric field. 1. Features of hydrodynamic interaction of polarized particles. Colloid J USSR 48:197–203

Gamayunov NI, Mantrov GI, Murtsovkin VA (1992) Study of flows induced in the vicinity of conducting particles by an external electric-field. Colloid J USSR 54:20–23

Gangwal S, Cayre OJ, Bazant MZ, Velev OD (2008) Induced-charge electrophoresis of metallodielectric particles. Phys Rev Lett 100:058302

García-Sánchez P, Ramos A, Green NG, Morgan H (2008) Traveling-wave electrokinetic micropumps: velocity, electrical current, and impedance measurements. Langmuir 24:9361–9369

Ghosal S (2003) The effect of wall interactions in capillary-zone electrophoresis. J Fluid Mech 491:285–300

Ghosal S (2004) Fluid mechanics of electroosmotic flow and its effect on band broadening in capillary electrophoresis. Electrophoresis 25:214–228

Ghowsi K, Gale RJ (1991) Field effect electroosmosis. J Chromatogr A 559:95–101

Gitlin I, Stroock AD, Whitesides GM, Ajdari A (2003) Pumping based on transverse electrokinetic effects. Appl Phys Lett 83:1486–1488

González A, Ramos A, Green NG, Castellanos A, Morgan H (2000) Fluid flow induced by nonuniform ac electric fields in

electrolytes on microelectrodes. II. A linear double-layer analysis. Phys Rev E 61:4019–4028

Goswami P, Chakraborty S (2009) Energy transfer through streaming effects in time-periodic pressure-driven nanochannel flows with interfacial slip. Langmuir 26:581–590

Green NG, Ramos A, González A, Morgan H, Castellanos A (2000) Fluid flow induced by nonuniform ac electric fields in electrolytes on microelectrodes. I. Experimental measurements. Phys Rev E 61:4011–4018

Green NG, Ramos A, González A, Morgan H, Castellanos A (2002) Fluid flow induced by nonuniform ac electric fields in electrolytes on microelectrodes. III. Observation of streamlines and numerical simulation. Phys Rev E 66:026305

Gregersen MM, Okkels F, Bazant MZ, Bruus H (2009) Topology and shape optimization of induced-charge electro-osmotic micropumps. New J Phys 11:075019

Guan W, Fan R, Reed MA (2011) Field-effect reconfigurable nanofluidic ionic diodes. Nat Commun 2:506

Halpern D, Wei HH (2007) Electroosmotic flow in a microcavity with nonuniform surface charges. Langmuir 23:9505–9512

Harnett CK, Templeton J, Dunphy-Guzman KA, Senousy YM, Kanouff MP (2008) Model based design of a microfluidic mixer driven by induced charge electroosmosis. Lab Chip 8:565–572

Heldal T, Volden T, Auerswald J, Knapp H (2007) Embeddable low-voltage micropump using electroosmosis of the second kind. In: 2007 NSTI Nanotechnology Conference and Trade Show. NSTI Nanotech 2007, Technical Proceedings, vol 3, Santa Clara, California, USA, pp 268–271

Herr AE, Molho JI, Santiago JG, Mungal MG, Kenny TW, Garguilo MG (2000) Electroosmotic capillary flow with nonuniform zeta potential. Anal Chem 72:1053–1057

Højgaard Olesen L, Bazant MZ, Bruus H (2010) Strongly nonlinear dynamics of electrolytes in large ac voltages. Phys Rev E 82:011501

Huang DM, Cottin-Bizonne C, Ybert C, Bocquet L (2008) Massive amplification of surface-induced transport at superhydrophobic surfaces. Phys Rev Lett 101:064503

Huang SH, Hsueh HJ, Hung KY (2010) Configurable AC electroosmotic generated in-plane microvortices and pumping flow in microchannels. Microfluid Nanofluid 8:187–195

Hunter RJ (1981) Zeta potential in colloid science. Academic Press, New York

Joly L, Ybert C, Trizac E, Bocquet L (2004) Hydrodynamics within the electric double layer on slipping surfaces. Phys Rev Lett 93:257805

Joseph P, Cottin-Bizonne C, Benoît JM, Ybert C, Journet C, Tabeling P, Bocquet L (2006) Slippage of water past superhydrophobic carbon nanotube forests in microchannels. Phys Rev Lett 97:156104

Joshi P, Smolyanitsky A, Petrossian L, Goryll M, Saraniti M, Thornton TJ (2010) Field effect modulation of ionic conductance of cylindrical silicon-on-insulator nanopore array. J Appl Phys 107:054701

Karnik R, Fan R, Yue M, Li D, Yang P, Majumdar A (2005) Electrostatic control of ions and molecules in nanofluidic transistors. Nano Lett 5:943–948

Karnik R, Castelino K, Majumdar A (2006) Field-effect control of protein transport in a nanofluidic transistor circuit. Appl Phys Lett 88:123114

Karnik R, Duan C, Castelino K, Daiguji H, Majumdar A (2007) Rectification of ionic current in a nanofluidic diode. Nano Lett 7:547–551

Khair AS, Squires TM (2009) The influence of hydrodynamic slip on the electrophoretic mobility of a spherical colloidal particle. Phys Fluids 21:042001

Kilic MS, Bazant MZ (2011) Induced-charge electrophoresis near a wall. Electrophoresis 32:614–628

Kilic MS, Bazant MZ, Ajdari A (2007) Steric effects in the dynamics of electrolytes at large applied voltages. I. Double-layer charging. Phys Rev E 75:021502

King BV, Freund F (1984) Surface charges and subsurface space-charge distribution in magnesium oxides containing dissolved traces of water. Phys Rev B 29:5814–5824

Kivanc FC, Litster S (2011) Pumping with electroosmosis of the second kind in mesoporous skeletons. Sens Actuators, B 151:394–401

Kline TR, Paxton WF, Wang Y, Velegol D, Mallouk TE, Sen A (2005) Catalytic micropumps: microscopic convective fluid flow and pattern formation. J Am Chem Soc 127:17150–17151

Kumar A, Qiu Z, Khusid B, Yeksel M, Acrivos A (2005) Strong DC and low-frequency AC fields for the manipulation of particles and fluids in microfluidics. 2005 NSTI Nanotechnology Conference and Trade Show—NSTI Nanotech 2005 Technical Proceedings, Anaheim, California, USA, pp 191–193

Lasne D, Maali A, Amarouchene Y, Cognet L, Lounis B, Kellay H (2008) Velocity profiles of water flowing past solid glass surfaces using fluorescent nanoparticles and molecules as velocity probes. Phys Rev Lett 100:214502

Lavrentovich OD, Lazo I, Pishnyak OP (2010) Nonlinear electrophoresis of dielectric and metal spheres in a nematic liquid crystal. Nature 467:947–950

Lee CS, Blanchard WC, Wu CT (1990) Direct control of the electroosmosis in capillary zone electrophoresis by using an external electric field. Anal Chem 62:1550–1552

Lee D-H, Farouk B, Noh H (2011) 3-D simulations of electroosmotic sample migration in microchannels: effects of surface and solution property variations. Sep Sci Technol 46:1377–1387

Leinweber FC, Tallarek U (2004) Nonequilibrium electrokinetic effects in beds of ion-permselective particles. Langmuir 20:11637–11648

Leinweber FC, Eijkel JCT, Bomer JG, Van Den Berg A (2006) Continuous flow microfluidic demixing of electrolytes by induced charge electrokinetics in structured electrode arrays. Anal Chem 78:1425–1434

Levich VG (1962) Physicochemical hydrodynamics. Prentice-Hall, Englewood Cliffs

Levitan JA, Devasenathipathy S, Studer V, Ben Y, Thorsen T, Squires TM, Bazant MZ (2005) Experimental observation of induced-charge electro-osmosis around a metal wire in a microchannel. Colloids Surf A 267:122–132

Loget G, Kuhn A (2010) Propulsion of microobjects by dynamic bipolar self-regeneration. J Am Chem Soc 132:15918–15919

Loget G, Kuhn A (2011) Electric field-induced chemical locomotion of conducting objects. Nat Commun 2:535

Long D, Ajdari A (1998) Symmetry properties of the electrophoretic motion of patterned colloidal particles. Phys Rev Lett 81:1529–1532

Long D, Stone HA, Ajdari A (1999) Electroosmotic flows created by surface defects in capillary electrophoresis. J Colloid Interface Sci 212:338–349

Lyklema J (1995) Fundamentals of interface and colloid science, vol 2. Academic Press, London

Macrae MX, Blake S, Mayer M, Yang J (2010) Nanoscale ionic diodes with tunable and switchable rectifying behavior. J Am Chem Soc 132:1766–1767

Mao P, Han J (2005) Fabrication and characterization of 20 nm planar nanofluidic channels by glass–glass and glass–silicon bonding. Lab Chip 5:837–844

Masliyah JH, Bhattacharjee S (2006) Electrokinetic and colloid transport phenomena. Wiley, Hoboken

Miloh T (2008) A unified theory of dipolophoresis for nanoparticles. Phys Fluids 20:107105

Mishchuk N, Gonzalez C, Takhistov P (2001) Electroosmosis of the second kind and current through curved interface. Colloids Surf A 181:131–144

Mishchuk NA, Heldal T, Volden T, Auerswald J, Knapp H (2009) Micropump based on electroosmosis of the second kind. Electrophoresis 30:3499–3506

Mittal M, Lele PP, Kaler EW, Furst EM (2008) Polarization and interactions of colloidal particles in ac electric fields. J Chem Phys 129:064513

Moorthy J, Khoury C, Moore JS, Beebe DJ (2001) Active control of electroosmotic flow in microchannels using light. Sens Actuators, B 75:223–229

Moran JL, Posner JD (2011) Electrokinetic locomotion due to reaction-induced charge auto-electrophoresis. J Fluid Mech 680:31–66

Morin FO, Gillot F, Fujita H (2007) Modeling the mechanisms driving ac electro-osmotic flow on planar microelectrodes. Appl Phys Lett 91:064103

Mpholo M, Smith CG, Brown ABD (2003) Low voltage plug flow pumping using anisotropic electrode arrays. Sens Actuators, B 92:262–268

Muller VM, Sergeeva IP, Sobolev VD, Churaev NV (1986) Boundary effects in the theory of electrokinetic phenomena. Colloid J USSR 48:606–614

Murtsovkin VA (1996) Nonlinear flows near polarized disperse particles. Colloid J Russ Acad Sci 58:341–349

Nadal F, Argoul F, Hanusse P, Pouligny B, Ajdari A (2002a) Electrically induced interactions between colloidal particles in the vicinity of a conducting plane. Phys Rev E 65:061409

Nadal F, Argoul F, Kestener P, Pouligny B, Ybert C, Ajdari A (2002b) Electrically induced flows in the vicinity of a dielectric stripe on a conducting plane. Eur Phys J E 9:387–399

Navier CLMH (1823) Mémoire sur les lois du mouvement des fluides. Mém Acad Roy Sci Inst France 6:389–440

Ng WY, Goh S, Lam YC, Yang C, Rodriguez I (2009) DC-biased AC-electroosmotic and AC-electrothermal flow mixing in microchannels. Lab Chip 9:802–809

Olga IV (1999) Slippage of water over hydrophobic surfaces. Int J Miner Process 56:31–60

Ou J, Perot B, Rothstein JP (2004) Laminar drag reduction in microchannels using ultrahydrophobic surfaces. Phys Fluids 16:4635–4643

Park HM, Kim TW (2009) Extension of the Helmholtz-Smoluchowski velocity to the hydrophobic microchannels with velocity slip. Lab Chip 9:291–296

Park S, Chung T, Kim H (2009) Ion bridges in microfluidic systems. Microfluid Nanofluid 6:315–331

Paxton WF, Baker PT, Kline TR, Wang Y, Mallouk TE, Sen A (2006) Catalytically induced electrokinetics for motors and micropumps. J Am Chem Soc 128:14881–14888

Perry JM, Zhou K, Harms ZD, Jacobson SC (2010) Ion transport in nanofluidic funnels. ACS Nano 4:3897–3902

Probstein RF (1994) Physicochemical hydrodynamics: an introduction. Wiley, New York

Ramos A, Morgan H, Green NG, Castellanos A (1998) Ac electrokinetics: A review of forces in microelectrode structures. J Phys D 31:2338–2353

Ramos A, Morgan H, Green NG, Castellanos A (1999) AC electric-field-induced fluid flow in microelectrodes. J Colloid Interface Sci 217:420–422

Ramos A, González A, Castellanos A, Green NG, Morgan H (2003) Pumping of liquids with ac voltages applied to asymmetric pairs of microelectrodes. Phys Rev E 67:056302

Rathore AS, Horvath C (1997) Capillary electrochromatography: theories on electroosmotic flow in porous media. J Chromatogr A 781:185–195

Ren Y, Stein D (2008) Slip-enhanced electrokinetic energy conversion in nanofluidic channels. Nanotechnology 19:195707

Ristenpart WD, Aksay IA, Saville DA (2003) Electrically guided assembly of planar superlattices in binary colloidal suspensions. Phys Rev Lett 90:128303

Ristenpart WD, Aksay IA, Saville DA (2007) Electrohydrodynamic flow around a colloidal particle near an electrode with an oscillating potential. J Fluid Mech 575:83–109

Rose KA, Meier JA, Dougherty GM, Santiago JG (2007) Rotational electrophoresis of striped metallic microrods. Phys Rev E 75:011503

Russel WB, Saville DA, Schowalter WR (1989) Colloidal dispersions. Cambridge University Press, Cambridge

Saintillan D, Darve E, Shaqfeh ESG (2006) Hydrodynamic interactions in the induced-charge electrophoresis of colloidal rod dispersions. J Fluid Mech 563:223–259

Sasaki N, Kitamori T, Kim HB (2006) AC electroosmotic micromixer for chemical processing in a microchannel. Lab Chip 6:550–554

Schasfoort RBM, Schlautmann S, Hendrikse J, Van Den Berg A (1999) Field-effect row control for microfabricated fluidic networks. Science 286:942–945

Sharp K, Yazdi S, Davison S (2011) Localized flow control in microchannels using induced-charge electroosmosis near conductive obstacles. Microfluid Nanofluid 10:1257–1267

Shiu J-Y, Kuo C-W, Chen P, Mou C-Y (2004) Fabrication of tunable superhydrophobic surfaces by nanosphere lithography. Chem Mater 16:561–564

Simonov IN, Dukhin SS (1973) Theory of electrophoresis of solid conducting particles in case of ideal polarization of a thin diffuse double-layer. Colloid J USSR 35:173–176

Siwy ZS (2006) Ion-current rectification in nanopores and nanotubes with broken symmetry. Adv Funct Mater 16:735–746

Sniadecki NJ, Lee CS, Sivanesan P, DeVoe DL (2004) Induced pressure pumping in polymer microchannels via field-effect flow control. Anal Chem 76:1942–1947

Soni G, Squires TM, Meinhart CD (2007) Nonlinear phenomena in induced charge electroosmosis. In: Proceedings of IMECE2007, ASME international mechanical engineering congress and exposition, Seattle, Washington, USA

Sparreboom W (2009) AC electroosmosis in nanochannels. PhD thesis, University of Twente, Enschede

Squires TM (2008) Electrokinetic flows over inhomogeneously slipping surfaces. Phys Fluids 20:092105

Squires TM, Bazant MZ (2004) Induced-charge electro-osmosis. J Fluid Mech 509:217–252

Squires TM, Bazant MZ (2006) Breaking symmetries in induced-charge electro-osmosis and electrophoresis. J Fluid Mech 560:65–101

Storey BD, Edwards LR, Kilic MS, Bazant MZ (2008) Steric effects on ac electro-osmosis in dilute electrolytes. Phys Rev E 77:036317

Stroock AD, Weck M, Chiu DT, Huck WTS, Kenis PJA, Ismagilov RF, Whitesides GM (2000) Patterning electro-osmotic flow with patterned surface charge. Phys Rev Lett 84:3314–3317

Takhistov P, Duginova K, Chang HC (2003) Electrokinetic mixing vortices due to electrolyte depletion at microchannel junctions. J Colloid Interface Sci 263:133–143

Talapatra S, Chakraborty S (2008) Double layer overlap in ac electroosmosis. Eur J Mech B 27:297–308

Teubner M (1982) The motion of charged colloidal particles in electric fields. J Chem Phys 76:5564–5573

Thamida SK, Chang HC (2002) Nonlinear electrokinetic ejection and entrainment due to polarization at nearly insulated wedges. Phys Fluids 14:4315–4328

Trau M, Saville DA, Aksay IA (1996) Field-induced layering of colloidal crystals. Science 272:706–709

Trau M, Saville DA, Aksay IA (1997) Assembly of colloidal crystals at electrode interfaces. Langmuir 13:6375–6381

Tsai P, Peters AM, Pirat C, Wessling M, Lammertink RGH, Lohse D (2009) Quantifying effective slip length over micropatterned hydrophobic surfaces. Phys Fluids 21:112002

Uppalapati M, Huang YM, Jackson TN, Hancock WO (2008) Microtubule alignment and manipulation using AC electrokinetics. Small 4:1371–1381

Van Der Wouden EJ, Hermes DC, Gardeniers JGE, Van Den Berg A (2006) Directional flow induced by synchronized longitudinal and zeta-potential controlling AC-electrical fields. Lab Chip 6:1300–1305

Vermesh U, Choi JW, Vermesh O, Fan R, Nagarah J, Heath JR (2009) Fast nonlinear ion transport via field-induced hydrodynamic slip in sub-20-nm hydrophilic nanofluidic transistors. Nano Lett 9:1315–1319

Vinogradova OI, Koynov K, Best A, Feuillebois F (2009) Direct measurements of hydrophobic slippage using double-focus fluorescence cross-correlation. Phys Rev Lett 102:118302

Vlassiouk I, Siwy ZS (2007) Nanofluidic diode. Nano Lett 7:552–556

Vlassiouk I, Smirnov S, Siwy Z (2008) Nanofluidic ionic diodes: comparison of analytical and numerical solutions. ACS Nano 2:1589–1602

Wang S, Feng L, Jiang L (2006) One-step solution-immersion process for the fabrication of stable bionic superhydrophobic surfaces. Adv Mater 18:767–770

Wu Z, Li D (2008) Micromixing using induced-charge electrokinetic flow. Electrochim Acta 53:5827–5835

Wu J, Ben Y, Battigelli D, Chang HC (2005) Long-range AC electroosmotic trapping and detection of bioparticles. Ind Eng Chem Res 44:2815–2822

Wu Z, Gao Y, Li D (2009) Electrophoretic motion of ideally polarizable particles in a microchannel. Electrophoresis 30:773–781

Yan R, Liang W, Fan R, Yang P (2009) Nanofluidic diodes based on nanotube heterojunctions. Nano Lett 9:3820–3825

Yang J, Kwok DY (2003) Effect of liquid slip in electrokinetic parallel-plate microchannel flow. J Colloid Interface Sci 260:225–233

Yariv E (2005) Induced-charge electrophoresis of nonspherical particles. Phys Fluids 17:1–4

Yeh SR, Seul M, Shraiman BI (1997) Assembly of ordered colloidal aggregates by electric-field-induced fluid flow. Nature 386:57–59

Yossifon G, Frankel I, Miloh T (2006) On electro-osmotic flows through microchannel junctions. Phys Fluids 18:117108

Yossifon G, Frankel I, Miloh T (2007) Symmetry breaking in induced-charge electro-osmosis over polarizable spheroids. Phys Fluids 19:068105

Yossifon G, Frankel I, Miloh T (2009) Macro-scale description of transient electro-kinetic phenomena over polarizable dielectric solids. J Fluid Mech 620:241–262

Zhang P, Qiu HH (2008) Investigation of the patterned surface modification on 3D vortex flow generation in a micropipe. J Micromech Microeng 18:115030

Zhang G, Wang D, Gu Z–Z, Möhwald H (2005) Fabrication of superhydrophobic surfaces from binary colloidal assembly. Langmuir 21:9143–9148

Zhao H (2010) Electro-osmotic flow over a charged superhydrophobic surface. Phys Rev E 81:066314

Zhao C (2012) Induced-charge nonlinear electrokinetic phenomena and applications in micro/nano fluidics. PhD thesis, Nanyang Technological University

Zhao H, Bau HH (2007) Microfluidic chaotic stirrer utilizing induced-charge electro-osmosis. Phys Rev E 75:066217

Zhao C, Yang C (2009) Analysis of induced-charge electro-osmotic flow in a microchannel embedded with polarizable dielectric blocks. Phys Rev E 80:046312

Zhao C, Yang C (2011a) AC electrokinetic phenomena over semiconductive surfaces: effective electric boundary conditions and their applications. Phys Rev E 83:066304

Zhao C, Yang C (2011b) AC field induced-charge electroosmosis over leaky dielectric blocks embedded in a microchannel. Electrophoresis 32:629–637

Zhao C, Yang C (2011c) On the competition between streaming potential effect and hydrodynamic slip effect in pressure-driven microchannel flows. Colloids Surf A 386:191–194

Zhao C, Yang C (2012) Electroosmotic flows in a microchannel with patterned hydrodynamic slip walls. Electrophoresis (To appear)

Zhu Y, Granick S (2001) Rate-dependent slip of newtonian liquid at smooth surfaces. Phys Rev Lett 87:096105

Zhu Y, Granick S (2002) Limits of the hydrodynamic no-slip boundary condition. Phys Rev Lett 88:106102